



Diurnal evolution of total column and surface atmospheric ammonia in the megacity of Paris, France, during an intense springtime pollution episode

5 Rebecca D. Kutzner¹, Juan Cuesta¹, Pascale Chelin¹, Jean-Eudes Petit^{2,3}, Mokhtar Ray¹, Xavier Landsheere¹, Benoît Tournadre^{1*}, Jean-Charles Dupont⁴, Amandine Rosso⁵, Frank Hase⁶, Johannes Orphal⁶, and Matthias Beekmann¹

¹ Laboratoire Interuniversitaire des Systèmes Atmosphériques (LISA), UMR CNRS 7583, Université Paris-Est
10 Créteil, Université de Paris, Institut Pierre Simon Laplace (IPSL), Créteil, France

² Laboratoire des Sciences du Climat et de l'Environnement, UMR 8212, CEA/Orme des Merisiers, 91191 Gif-sur-Yvette, France

³ INERIS, Parc Technologique ALATA, 60750 Verneuil-en-Halatte, France

⁴ Institut Pierre-Simon Laplace, École Polytechnique, UVSQ, Université Paris-Saclay, 91128 Palaiseau, France

15 ⁵ AIRPARIF, Agence de surveillance de la qualité de l'air, Paris, France

⁶ Institut für Meteorologie und Klimaforschung (IMK), Karlsruher Institut für Technologie (KIT), Karlsruhe, Germany

*New affiliation: Centre for Observation, Impacts, Energy, Mines ParisTech, Sophia Antipolis Cedex, France

20 *Correspondence to:* Rebecca D. Kutzner (rebecca.kutzner@lisa.u-pec.fr) and Pascale Chelin (pascale.chelin@lisa.u-pec.fr)

Abstract. Ammonia (NH₃) is a key precursor for the formation of atmospheric secondary inorganic particles, such as ammonium nitrate and sulfate. Although the chemical processes associated with the gas-to-particle conversion are well known, atmospheric concentrations of gaseous ammonia are still scarcely characterized. This information is however critical especially for processes concerning the equilibrium between ammonia and ammonium nitrate, due to the semi-volatile character of the latter one. This study presents an analysis of the diurnal cycle of atmospheric ammonia during a pollution event over the Paris megacity region in spring 2012 (five days in late March 2012). Our objective is to analyze the link between the diurnal evolution of surface NH₃ concentrations and its integrated column abundance, meteorological variables and relevant chemical species involved in gas/particle partitioning. For this, we implement an original approach based on the combined use of surface and total column ammonia measurements. These last ones are derived from ground-based remote sensing measurements performed by the “Observations of the Atmosphere by Solar Infrared Spectroscopy” (OASIS) Fourier transform infrared observatory at an urban site over the southeastern suburbs of the Paris megacity. This analysis considers the following meteorological variables relevant to the ammonia pollution event: temperature, relative humidity, wind speed and direction and vertical dilution in the atmospheric boundary layer. Moreover, we study the partitioning between ammonia and ammonium particles from concomitant measurements of total particulate matter (PM) and ammonium (NH₄⁺) concentrations at the surface. We identify the origin of the



pollution event as local emissions at the beginning of the analyzed period and advection of pollution from the
40 Benelux and west Germany by the end. Our results show a clearly different diurnal behavior of atmospheric
ammonia concentrations at the surface and those vertically integrated over the total atmospheric column. Surface
concentrations remain relatively stable during the day, while total column abundances show a minimum value in
the morning and rise steadily to reach a relative maximum in the late afternoon during each day of the spring
pollution event. These differences are mainly explained by vertical mixing within the boundary layer, as suggested
45 by ground-based measurements of vertical profiles of aerosol backscatter, used as tracer of the vertical distribution
of pollutants in the atmospheric boundary layer. Indeed, the afternoon enhancement of ammonia clearly seen by
OASIS for the whole atmospheric column is barely depicted by surface concentrations, as the latter are strongly
affected by vertical dilution within the rising boundary layer. Moreover, the concomitant occurrence of a decrease
50 of ammonium particle concentrations and an increase of gaseous ammonia abundance suggests the volatilization
of particles for forming ammonia. Furthermore, surface observations may also suggest night-time formation of
ammonium particles from gas-to-particle conversion, for relative humidity levels higher than the deliquescence
point of ammonium nitrate.

1. Introduction

55 Ammonia (NH_3) is a harmful air pollutant that directly affects human health and also contributes to intense smog
events through the neutralization of sulfuric and nitric acids for forming secondary aerosols such as ammonium
sulfate ($(\text{NH}_4)_2\text{SO}_4$) and nitrate (NH_4NO_3) (Behera et al., 2013, Seinfeld and Pandis, 2016, Elster et al., 2018).
These particles can be transported over long distances and contribute to the degradation of air quality and the
eutrophication of water bodies. Volatilization of ammonium nitrate particles forms gaseous ammonia depending
60 on atmospheric temperature (T), relative humidity (RH) and the pH of the particles e.g. (Seinfeld and Pandis,
2016; Weber et al., 2016; Guo et al., 2018). Through conversion into different forms of reactive nitrogen, further
impacts of ammonia are directly or indirectly linked to acidic precipitation, causing eutrophication and a decrease
in biodiversity (Sutton et al., 2013, Krupa, 2003).

65 The main source of NH_3 in Europe is the agricultural sector with an average of 92 % of total ammonia emission
(<https://data.europa.eu/>). It is emitted by volatilization from fertilizer storage, livestock as well as manure and
mineral nitrogen fertilizers applied on crops, as a function of temperature, windspeed and atmospheric stability
e.g. (Sommer et al., 2004, Behera et al., 2013). Other emissions are associated with traffic and industry. In France,
the dominant source of NH_3 is also attributed to the agricultural sector, with contributions between 94 % to 98 %,
70 among which 50 % is due to nitrogen-based fertilizers as well as emissions from livestock (Génermont et al.,
2018, Ramanantenasoa et al., 2018). In many regions of Africa, Inner Mongolia, South Siberia and South America,
fires are another anthropogenic source of NH_3 (Behera et al., 2013). Natural sources are related to biological
mechanisms in soils, plants and soil-plant interaction, as described in detail by Behera et al. (2013).

The European Union (EU) addressed ammonia emission in the National Emission Ceilings Directive 2001/81/EC
75 (NECD). Serrano et al. (2019) recently reviewed reduction efforts of nitrogen levels between 2001 and 2011,
finding a significant impact of ammonia emitted from agriculture on ecosystems. Exceedances of ammonia
emissions compared to ceilings set for 2010 are still occurring (NEC Directive reporting status 2018). New



reduction goals for the period of 2020 to 2029 and a second period after 2030 are set for each European country in the DIRECTIVE (EU) 2016/2284.

80 Pollution events in urban areas directly impact human health and greatly reduce visibility e.g. Molina and Molina (2004). This recurrently occurs during springtime over the Paris megacity (12.2 million inhabitants including suburbs) and other European megacities due to emissions from agricultural activities in the areas surrounding the agglomerations e.g. Petit et al. (2015). Accurate and long-term measurements of atmospheric pollutants, such as ammonia, and meteorological conditions are crucial in order to better understand the origin and the evolution of

85 these pollution events. In the Paris region, springtime is a very propitious period for particulate matter pollution episodes, essentially dominated by secondary inorganic aerosols, such as ammonium nitrate and sulfate (Sciare et al., 2011, Petit et al., 2015). Concomitantly, ammonia concentrations have been found exceptionally high, as reported by surface in-situ measurements (Petit et al., 2015; Petetin et al., 2016) and remote sensing from the ground and satellite (Tournadre et al., 2020; Viatte et al., 2020). Indeed, that period of the year is characterized

90 by fertilizer spreading, which can dramatically enhance NH_3 emissions (Ramanantenasoa et al., 2018). Different techniques are used to measure concentrations of NH_3 in the atmosphere. Accurate in situ measurements of ammonia are difficult due a “sticky” nature, as it accumulates in the inlets and sampling tubes (Yokelson et al., 2003). In order to reduce these artefacts, different techniques are often implemented, such as Teflon or halocarbon wax coating to diminish the accumulation of ammonia and a heating system to reduce relative humidity (RH) that

95 can lead to sampling biases by losses of NH_3 (Yokelson et al., 2003). Remote sensing of ammonia is an innovative alternative to in situ techniques, which offers a significant enhancement of spatial coverage. Satellite approaches are currently based on hyper spectral thermal infrared measurements from the Cross-track Infrared Sounder (CrIS, Shephard and Cady-Pereira, 2015) and the Infrared Atmospheric Sounding Interferometer (IASI, Clerbaux et al., 2009), respectively onboard the United States Suomi

100 National Polar Partnership (SNPP) and the European MetOp satellites. Both platforms are pointing nadir in polar sun-synchronous orbits, with overpasses around 09:30 and 21:30 local time (LT) for IASI and 13:30 and 01:30 LT for CrIS (Shephard and Cady-Pereira, 2015, Dammers et al., 2017). Therefore, they both offer global coverage twice a day, providing particularly valuable measurements over remote regions lacking of ground-based instruments such as in the tropics. Remote sensing of ammonia can also be performed using hyperspectral

105 measurements from a ground-based Fourier-transform infrared (FTIR) spectrometer, like the OASIS (Observations of Atmosphere by Solar Infrared Spectroscopy, Chelin et al., 2014) mid-resolution observatory in Créteil (France). Remote sensing from satellite and ground-based platforms provides vertically integrated amounts of ammonia over the atmospheric column for cloud-free conditions. The combined use of remote sensing and in situ measurements offers an interesting framework for analyzing ammonia variability both at the surface and

110 integrated over the atmospheric column, as already done for greenhouse gases (Zhou et al., 2018). FTIR ground-based measurements can provide highly valuable information on the diurnal evolution of atmospheric species for a particular geographical location, as shown here for ammonia at the Paris suburbs. Although numerous FTIR ground-based stations currently exist, such as those of the NDACC network (De Mazière et al., 2018), only few of them document the diurnal evolution of atmospheric constituents.

115

This paper presents a detailed analysis of the diurnal evolution of ammonia as observed in total columns from ground-based remote sensing and at the surface from an in-situ analyzer in Paris, France, during a major pollution



event in late March 2012. We characterize the diurnal variation of ammonia, analyzing both the link with the formation and volatilization of ammonium particles and vertical dilution in the atmospheric boundary layer. Spring 2012 was one of the most polluted periods since 2007, with a succession of persistent pollution events (Petit et al., 2015, Petit et al. 2017). We use total column ammonia concentrations derived from OASIS observatory at southeast Paris suburbs (Créteil) and surface observations at southwest Paris suburbs (Palaiseau) to characterize the diurnal evolution of ammonia between 26 and 30 March 2012. To the authors' knowledge, this is the first analysis of the diurnal evolution of ammonia from both total column and surface measurements, in close relation with particle phase measurements.

Section 2 provides information concerning the instruments from the OASIS and SIRTAs sites, as well as other datasets used for this study. We also provide a brief description of the new retrieval of ammonia from OASIS (Tournadre et al., 2020). In the third section, we present and discuss the analysis of these datasets. First, we describe the regional conditions of the Paris pollution event in late March 2012 using meteorological analysis, a chemistry-transport model and satellite data (Sect. 3.1). Then, we analyze the diurnal evolution of surface and total columns of ammonia and particular matter as well as meteorological variables over the Paris region (Sect. 3.2 to 3.4). Following, we analyze the complementarity of surface and total column measurements of ammonia using ground-based backscatter lidar (Light Detection And Ranging) measurements, as proxy for the vertical distribution of pollutants within the atmospheric boundary layer (Sect. 3.5). Section 4 provides conclusions of this study.

2. Datasets

2.1 Description of ground-based sites and platforms

An original aspect of this work is the analysis of the diurnal evolution of total column observations of ammonia derived from OASIS. This remote sensing observatory is located in Créteil (OASIS; 48.79° N, 2.44° E; 56 m above sea level (asl)), at the southeast suburbs of Paris, on the rooftop of the Université Paris-Est Créteil (UPEC, Chelin et al. 2014). It is an urban site mainly affected by background levels of pollution (Figure 1).

Measurements from other sites over the Paris region are also used in the current study (Figure 1). Meteorological and detailed atmospheric composition data at the surface level are measured at the “Site Instrumental de Recherche par Télédétection Atmosphérique” supersite near Palaiseau (SIRTA; 48.72° N, 2.20° E; <http://sirta.ipsl.fr>), located about 19 km southwest from OASIS and southwest Paris, which is often used for monitoring background air quality conditions of the Paris region (Haefelin et al., 2005). We use radiosounding measurements of temperature, pressure and humidity profiles from the Trappes station about 31 km west of Créteil, 15 km away from the SIRTA supersite and operated by Météo France. Additional surface measurements of PM_{2.5} and PM₁₀ (particle matter with aerodynamic diameter respectively less than 2.5 and 10 μm) are provided by the Airparif network dedicated to monitoring air quality in the Paris region (<https://www.airparif.asso.fr/>) from the stations of Vitry-sur-Seine, Bobigny and Gennevilliers. In the paper, time series of measurements are presented in terms of hourly median values, except stated otherwise.



2.2 Observations of total column ammonia derived from OASIS

155 Since 2009, the OASIS observatory regularly records high spectral measurements of solar radiation absorbed and scattered by atmospheric constituents, under clear-sky conditions (Chelin et al. 2014). It uses a mid-spectral resolution Fourier-transform spectrometer manufactured by Bruker Optics (the Vertex 80 model) with a spectral resolution of 0.06 cm^{-1} (corresponding to a maximum optical path difference of 12 cm). OASIS is routinely used for monitoring air pollutants, such as tropospheric ozone (O_3) and carbon monoxide (CO), with good accuracy and high sensitivity to near surface concentrations (Viatte et al., 2011). This system is particularly suited for air quality monitoring in megacities, given its compactness and moderate cost and it can play a key role in validating current (e.g. IASI) and future satellite observations (e.g. Infrared Atmospheric Sounder Interferometer Next Generation - IASI-NG and the InfraRed Sounder onboard the Meteosat Third Generation mission - MTG/IRS). The observatory is covered by an automatized cupola (Sirius 3.5 “School Model” observatory, 3.25 m high and 165 3.5 m in diameter), in which the aperture rotates for tracking the solar position. The altitude-azimutal solar tracker of OASIS uses bare gold-coated mirrors (A547N model from Bruker Optics). Infrared solar radiation spectra are recorded by a DTGS (deuterated triglycine sulphate) detector using a potassium bromide (KBr) beamsplitter to cover the large spectral region from 700 to 11000 cm^{-1} ($0.9\text{--}14.3\text{ }\mu\text{m}$) with no optical filter. The acquisition system is set to co-add 30 scans at maximum spectral resolution in order to provide atmospheric spectra every 10 minutes 170 (the temporal resolution of OASIS data). Absolute calibration of spectra measured by OASIS is done every month with a reference internal source of radiation.

Ammonia concentrations integrated over the total atmospheric column are retrieved with the PROFFIT 9.6 code developed by the Karlsruhe Institute of Technology (Germany, Hase et al., 2004), adapted for the medium spectral resolution. As detailed by Tournadre et al. (2020), two spectral micro-windows within the ν_2 vibrational band of 175 NH_3 are used: $926.3\text{--}933.9\text{ cm}^{-1}$ and $962.5\text{--}970\text{ cm}^{-1}$. The main interfering species in this spectral range are water vapour (H_2O), carbon dioxide and O_3 , whose abundances are jointly adjusted with that of NH_3 . We also use climatological concentrations for minor interfering gases (i.e. nitric acid HNO_3 , sulphur hexafluoride SF_6 , ethane C_2H_6 , and chlorofluorocarbons - CFC-12). The spectral signatures of absorption of infrared radiation by ammonia is clearly seen in individual spectra measured by OASIS, such as those recorded during a pollution event during 180 March 2012 (as compared to the atlas from Meier et al. (2004), see Fig. 2). Atmospheric columns of ammonia derived from the 9 year-database of OASIS range from $0.0005\text{ }10^{16}$ to $9\text{ }10^{16}$ molecules per square centimetre (molec.cm^{-2}) and their retrieval error is estimated to 20-35% (Tournadre et al., 2020). OASIS retrievals of NH_3 total columns show a good agreement with co-located observations derived from IASI (the ANNI-NH3-v2.2R version, Van Damme et al., 2017): a linear correlation coefficient of ~ 0.8 and a small mean difference of ~ 0.08 185 $10^{16}\text{ molec.cm}^{-2}$, with OASIS-derived concentrations slightly larger (Tournadre et al., 2020). This last aspect could be associated with an enhanced sensitivity to larger concentrations of NH_3 near the surface for OASIS, as compared to the satellite retrieval which is most sensitive for higher atmospheric layers.

2.3 Surface in situ observations of ammonia and aerosol composition

In the present analysis, we use in situ gaseous ammonia measurements at surface level carried out with an 190 AiRRmonia instrument (Mechatronics Instruments, the Netherlands) at the SIRTA observatory (Haeffelin et al., 2005). The principle of this instrument, described in Cowen et al. (2004), is essentially based on conductimetric



detection of ammonia dissolved in water (i.e. in the form of ammonium), and has been shown from several intercomparison exercises to provide accurate NH_3 measurements (Norman et al., 2009, von Bobruzki et al., 2010). The AiRRmonia was regularly calibrated with 0 and 500 ppb ammonium solution.

195 Concomitant measurements of the major chemical composition of submicron aerosols were performed with an Aerosol Chemical Speciation Monitor (ACSM, Aerodyne Research Inc., Billerica, MA, USA; Ng et al., 2011), providing concentrations of particulate organic matter (OM), nitrate (NO_3^-), sulphate (SO_4^{2-}), ammonium (NH_4^+) and chloride (Cl^-), every 30 minutes. Submicron particles are sampled at 3 l min^{-1} , subsampled at 0.85 l min^{-1} , and focused through an aerodynamic lens for PM_{10} (particle matter with aerodynamic diameter smaller than $1 \mu\text{m}$).

200 Non-refractory particles are then flash-vaporized on a 600°C -heated plate, fragmented by electronic impact at 70 keV, and eventually separated and detected by a quadrupole. Calibrations were performed by injecting known concentrations of ammonium nitrate and ammonium sulfate particles with an aerodynamic diameter of 300 nm. Details on the operational conditions of the AiRRmonia and the ACSM instruments at SIRTAs are provided by Petit et al. (2015).

205 As observed by Petit et al. (2015), we expect the daily evolution of ammonia over the Paris region to be closely linked to the gas to particle conversion between ammonia (gas) and ammonium nitrate particles. This is a reversible conversion for which the equilibrium is closely linked to the abundance of precursors (NH_3 and HNO_3), and meteorological conditions, temperature and relative humidity (Seinfeld and Pandis, 2016). Pre-conditions for volatilization of NH_3 from NH_4NO_3 are given by the relationship of relative humidity and deliquescence relative

210 humidity (DRH), which depends on the temperature. Whereby volatilization is favored when RH is much lower than DRH. In order to estimate the balance between DRH and RH, we consider following equation, as suggested by Seinfeld and Pandis (2016):

$$DRH(T) = DRH(298) \exp \left\{ \frac{\Delta H_S}{R} \left[A \left(\frac{1}{T} - \frac{1}{298} \right) - B \ln \frac{T}{298} - C(T - 298) \right] \right\}$$

DRH(298) is the deliquescence relative humidity of NH_4NO_3 at 298 K, which corresponds to 61.8 %. ΔH_S is the enthalpy of solution for NH_4NO_3 at 298 K which is $25.69 \text{ kJ mol}^{-1}$, R is the universal gas constant, T is the temperature in K. A, B, and C are factors for the solubility of common aerosol salts in water as a function of temperature provided by Seinfeld and Pandis (2016) (i.e. 4.3, $-3.6 \cdot 10^{-2}$ and $7.9 \cdot 10^{-5}$ respectively). Moreover, partitioning between ammonia and ammonium nitrate is also influenced by the pH of the ambient particles (e.g. Weber et al., 2016; Guo et al., 2018). When pH drops below an approximate critical value of 3 (slightly higher in

220 warm and slightly lower in cold seasons), the NH_3 reduction leads to evaporation of NH_4NO_3 , while this is not expected to happen for moderately acid to neutral conditions.

2.4 Regional conditions from satellite data and models

For characterizing the pollution event during March 2012, we use a suite of satellite and model datasets concerning

225 both the pollutant distributions at regional and continental scale and meteorological conditions. Aerosol optical depth (AOD) derived from satellite and ground-based measurements are used for analyzing the spatial and temporal evolution of total particle abundance integrated over the atmospheric column. The horizontal distribution of AOD over western Europe is described using MODIS (Moderate Resolution Imaging Spectroradiometer, Remer et al., 2005) data onboard the Terra (MOD04L2) satellite with overpasses at 10:30 LT (from the NASA



230 worldview website <https://worldview.earthdata.nasa.gov/>; Levy, R., and Hsu, C., 2015). The MODIS images have
a horizontal resolution of 3 km at nadir.

The horizontal distribution of air pollutants at the European scale is also studied with CHIMERE chemistry-
transport model simulations (Menut et al., 2013) from the inter-regional platform Esmeralda (EtudeS Multi
RégionALes De l'Atmosphère, <http://www.esmeralda-web.fr>, Cortinovis et al., 2015). This model is run hourly
235 and averaged at daily scale, with a horizontal resolution of 15 x 15 km² and 8 vertical levels between 40 m to 5
km. Ammonia, nitrate and sulfate exist in aqueous, gaseous and particulate phases in the model. Equilibrium
between dissolved gases concentration and gas-phase concentrations follow (Seinfeld and Pandis, 2016).

Meteorological conditions are analyzed from in-situ measurements and numerical model simulations. We use sea-
level pressure, wind and potential temperature fields from ERA-Interim (ERA-Interim, Simmons et al., 2007) reanalyzes
240 of the European Centre for Medium-Range Weather Forecasts (ECMWF) that are provided by the Institut Pierre
Simon Laplace mesocentre (<https://mesocentre.ipsl.fr>). These simulations have a 0.75 x 0.75° horizontal
resolution and 37 pressure levels.

2.5 Local conditions at the Paris region from ground-based measurements

245

Meteorological conditions at the surface over the Paris region are analyzed by in situ measurements of wind speed
and direction performed at the SIRTA site (Haefelin et al., 2005). Local temperature and relative humidity were
measured at Créteil with a LOG 110-EXF sensor, with an accuracy in temperature of $\pm 0.5^{\circ}\text{C}$ and in relative
humidity of $\pm 3\%$.

250 Vertical profiles of temperature and relative humidity from the surface up to 25 km of altitude and with about 10-
m vertical resolution are measured by radiosoundings launched around noon and mid-night at the Trappes site (at
southwest suburbs of Paris).

The diurnal evolution of particle pollution over the Paris region is studied in terms of surface measurements of
PM_{2.5} and PM₁₀ from several Airparif sites and AOD measured by ground-based sun photometers (version 3 of
255 level 2.0 data) at the Paris and SIRTA sites from the AERONET (Aerosols Robotic Network, Holben et al., 2001,
<https://aeronet.gsfc.nasa.gov/>) network. We use the distinction between AOD from a fine (e.g. smoke or smog)
and coarse (e.g. sea-salt or dust) mode at 500 nm, derived from the wavelength dependence of the AOD (O'Neill
et al., 2003; Giles et al., 2019). Errors in AOD data correspond to approximately 0.02 (Giles et al., 2019).

260 Additionally, we use ground-based lidar measurements from the SIRTA site for describing the vertical distribution
of particles over the Paris region, which is used as an indicator of the vertical distribution of air pollutants and the
vertical structure of the atmospheric boundary layer. This is done with vertical profiles of attenuated backscatter
profiles, measured by an elastic backscatter lidar (the ALS model manufactured by Leosphere) at 355 nm. The
mixing boundary layer height is manually identified as the lowest marked discontinuity of the lidar profiles during
daytime hours (from 06:00 to 18:00 UTC).

265



3. Results

We focus our study on the diurnal evolution of ammonia during a major pollution event over the Paris region occurring at the end of March 2012. It corresponds to the period with highest concentrations of ammonia on the multiyear time series (2009–2017) of OASIS measurements, which is probably linked to the springtime spreading
270 of mineral fertilizer in the Paris region and the surrounding regions (Ramanantenasoa et al., 2018; Tournadre et al., 2020). It is the most polluted spring season between 2007 and 2015 (Petit et al., 2017).

3.1. Meteorological and atmospheric conditions over western Europe

During late March 2012, the prevailing atmospheric conditions over western Europe are driven by an anticyclonic high-pressure system centered over Great Britain and the North Sea (55°N, 0°E) on 26 March and moving
275 westwards in the following days (see Fig. 3a, d, g). Following the anticyclonic circulation associated with this system, north-easterly winds blow from the Benelux region (Belgium, Netherlands and Luxembourg) to northern France. As expected for an anticyclonic period, relatively low wind speeds occur at its core, located over central Europe (from southern France to eastern Germany), which are accompanied by high insolation and low cloudiness (not shown). According to MODIS satellite observations (Fig. 3b, e, h) and CHIMERE simulations (Fig. 3c, f, i),
280 an aerosol plume with moderate AOD (0.2 to 0.3) and moderately large concentrations of PM_{2.5} at the surface (20 to 30 µg m⁻³) is formed on 26 March over the Benelux and extends across the English Channel. Meanwhile, aerosol baseline levels are observed over northern France (AOD ~0.1 and 10–15 µg m⁻³ for surface PM_{2.5}). After 27 March, the aerosol plume reaches northern France and southern England. On 28 March, a clear enhancement of the aerosol load over the Benelux and northern France is observed both in terms of AOD (up to 0.4) and surface
285 PM_{2.5} concentrations (up to 50 µg m⁻³). These high aerosol loads over northern France remain until 30 March (not shown). Both the horizontal extent of the aerosol plume and wind directions suggest that these highly polluted air masses originate over the Benelux as well as west Germany and are transported southwestwards, clearly reaching the Paris region after 28 March (also remarked for this pollution event by Fortems-Cheiney et al., 2016).

3.2 Geographical distribution of particle matter over the Paris region

290 Over the Paris region, particle concentrations at the surface are moderately high on 26–27 March (PM_{2.5} concentrations up to 40 µg m⁻³, see surface measurements of PM levels from several stations of the Paris region in Fig. 4). As polluted air masses are advected from the Benelux and west Germany on 28–29 March, PM_{2.5} levels clearly enhance (up to 80 µg m⁻³). Figure 4 also shows the largest peaks of surface PM_{2.5} concentrations occurring every day during the morning and secondary high values in the late evening.
295 Very similar temporal evolutions of surface particle concentrations are observed over the whole Paris region and during the entire period (26–30 March), both in absolute and relative terms. Figure 4 illustrates this horizontally homogenous distribution of surface PM as the chosen stations are located at the southeast, southwest, northeast and northwest suburbs of Paris (Fig. 1). The same peaks and troughs of surface PM are seen for all these locations. Particularly, we also remark that PM₁ at SIRTa also shows the same temporal evolution as other stations in the
300 Paris region, but with levels roughly ~30% below those of PM_{2.5} on 26–28 March and similar concentrations afterwards (for both PM₁ and PM_{2.5}). The clear similarity of these measurements at four different locations of the Paris suburbs suggests that we may also expect a consistent evolution of pollution levels at the Créteil site (OASIS



observatory), whose observations are also used later in this section for analyzing the evolution of the atmospheric ammonia concentrations during the event.

305 The time series of surface PM levels suggest the occurrence of 2 distinct pollution regimes within the period of 26-30 March. Indeed, while daily mean $PM_{2.5}$ values on 26-27 March remain under the air quality 24 h guideline of WHO (World Health Organization, $PM_{2.5}$ of $25 \mu\text{g m}^{-3}$, except for one station on one day), this $PM_{2.5}$ threshold is exceeded for all stations on 28-30 March. Hereafter, we denominate these two regimes as: period 1 or P1 (26-27 March) and period 2 or P2 (28-30 March). These two different atmospheric conditions are also pointed out by

310 Petit et al. (2015) by analyzing this particular pollution episode using surface measurements at SIRTA. A statistical comparison of the similarity of surface PM measurements from different sites over the Paris region is shown in Table 1 (for periods 1 and 2). For the first period (26-27 March), the time series of hourly $PM_{2.5}$ measurements performed at three different locations show a moderate correlation between each other (R^2 of 0.63 to 0.67), suggesting a similar evolution but with some horizontal heterogeneity over the Paris region. During the

315 second period (28-30 March), correlations between PM measurements are clearly higher (R^2 of 0.86 to 0.91) and therefore indicate a more horizontally homogenous PM distribution over the Paris region. Levels of surface PM_{10} for the same stations and periods show similar behaviors (Table 1). This different behavior between P1 and P2 is likely linked to the origin of the pollution event, being rather local for P1 and dominant advection of air pollution from the Benelux during P2, as remarked in the regional analysis of AOD, PM and wind regimes of section 3.1.

320 Additionally, we note that comparisons of $PM_{2.5}$ from 3 stations to PM_1 at SIRTA show moderate correlations during P1 as the other measurements, but lower ones during P2 (although peaks and troughs are clearly coincident).

3.3 Evolution of ammonia concentrations over the Paris region

During the periods P1 and P2, ammonia concentrations over the Paris region are observed both at surface level

325 (using in situ analyzer at SIRTA) and integrated over the total atmospheric column (using OASIS at Créteil, Fig. 5). Total atmospheric columns of NH_3 show a very marked and clear diurnal evolution: lower column amounts of ammonia in the morning that rise almost monotonically during the day until reaching a maximum in the afternoon. Both on 26 and 27 March, stable ammonia concentrations around $2 \cdot 10^{16} \text{ molec.cm}^{-2}$ remain until noon and then increase only in the afternoon. Early morning total columns of NH_3 on 28 and 29 March are lower (respectively

330 $1.4 \cdot 10^{16}$ and $0.6 \cdot 10^{16} \text{ molec.cm}^{-2}$) than for the previous days and show a steady enhancement from the early morning to the afternoon. The highest total column of ammonia is measured on 28 March ($4.6 \cdot 10^{16} \text{ molec.cm}^{-2}$). On 30 March, the diurnal evolution of NH_3 total columns is more similar to the first two days (26-27 March). Steady total columns around $1.5 \cdot 10^{16} \text{ molec.cm}^{-2}$ during the first 1.5 hours of the morning are followed by a decrease down to $0.85 \cdot 10^{16} \text{ molec.cm}^{-2}$ around 11:00 UTC and afterwards an increase up to $2.5 \cdot 10^{16} \text{ molec.cm}^{-2}$,

335 which is lower than those observed during the previous 4 days. This clear enhancement of ammonia total atmospheric columns during the day measured by OASIS is found typical of springtime polluted periods as already analyzed by Tournade et al. (2020) but not showed here (e.g. in March 2014, and March 2016). For all these years, the NH_3 maximum in the afternoon is above $2 \cdot 10^{16} \text{ molec.cm}^{-2}$ (Tournadre et al., 2020).

Meanwhile, surface measurements at SIRTA show relatively high overall levels of ammonia: from 2 to $10 \mu\text{g m}^{-3}$

340 3 , which is higher than Paris urban background levels of 1-3 $\mu\text{g m}^{-3}$ shown by Petetin et al. (2016), but for a May 2010 to February 2011 period. On each of the days of the event (26-30 March), morning daily maxima (up to 6-9



$\mu\text{g m}^{-3}$) and smaller evening peaks (around $5 \mu\text{g m}^{-3}$, Fig. 5) are clearly depicted. Although both surface (Fig. 5b) and integrated total column (Fig. 5a) ammonia measurements show large concentrations, their daily evolutions are clearly different. While total column values increase steadily during the day until reaching a peak in the late afternoon, surface ammonia moderately fluctuates during the day. These differences may be associated with atmospheric processes or interactions with the surface that modify ammonia concentrations differently as a function of altitude. This may be the case for vertical dilution of atmospheric constituents within the atmospheric boundary layer or the vertical variability of gas/particle partitioning related to relative humidity, temperature and particle pH. These aspects are investigated in detail in the following paragraphs.

Vertical variations of atmospheric ammonia concentrations may potentially be associated with temperature and relative humidity vertical profiles. As mentioned in Sect. 2.3, dry conditions lead to volatilization of ammonia from ammonium particles, whereas humidity levels beyond the deliquescence point favor the inverse process (Seinfeld and Pandis, 2016). During the pollution event on 26-30 March, temperature shows the usual steady decrease with altitude from the surface until the tropopause (see the median temperature profile measured by radiosoundings launched at Trappes on 26-30 March, Fig. 6a). Relative humidity varies greatly at the lowest few kilometers of the atmosphere, typically increasing with altitude within the mixing boundary layer (up to 1 to 1.5 km above sea level, asl, for the present case, see Fig. 6b). On 26-27 and 29 March, relative humidity increases from 25 % at the surface up to 35-40 % around 900 m asl and drops above 1000 m asl down to 10-20 %. On 28 March, relative humidity is roughly 15 % higher than on the mentioned days up to 800 m asl, above which it decreases down to 48 % and then rises up to 60 % at 1600 m asl, dropping down to 30 % at 2500 m asl. In all these cases, relative humidity up to 2500 m asl remains below the deliquescence point (DRH) as shown in Fig. 6b, thus favouring the formation of NH_3 by volatilization of ammonium particles. This is also confirmed by relative humidity time series at different altitudes (200, 500 and 1000 m asl), reconstructed from all radiosounding measurements over the entire event (launched from Trappes both at mid-day and mid-night, Fig. 6c). This supports a hypothesis of an increase in ammonia amounts due to volatilization of ammonium nitrate at higher altitudes. Relative humidity always remains below the DRH (grey band), except for one single measurement at 1000 m on 30 March at noon. We also remark that during the whole period relative humidity does not vary much vertically below 1000 m (except on 30 March) and that the most humid conditions are found at mid-nights from 28 to 30 March. No contrasting conditions between mid-day and mid-night are either found for the vertical shape of relative humidity. We do not clearly point out any particular link or concomitant temporal variation of relative humidity every 12 h at different altitudes (Fig. 6c) and ammonia measurements (Fig. 5).

An additional analysis was performed with the ISORROPIA II box model (Nenes et al., 1998) to investigate the role of temperature and relative humidity in the partitioning of ammonium nitrate. Results indicate that as expected the partitioning of ammonia into the particulate phase is favored with the decrease of temperature. This temperature decrease is correlated to an increase of relative humidity (while values remaining below DRH). Therefore, in equilibrium conditions (e.g. in absence of ammonia and ammonium advection), a vertically decreasing variation of ammonia with increasing altitudes likely occurs for these atmospheric conditions. Nevertheless, it should be noted that pH and aerosol chemical composition also impact ammonium nitrate partitioning. PM_{10} was found to be neutralized during the period study (Figure S1 in the supplementary material), therefore we expect a limited influence of ambient particle pH. However, our full understanding is limited by the lack of HNO_3 in-situ and column measurements.



As a conclusion, the decrease in T and the increase of RH for higher altitudes with respect to ground shift the equilibrium to the aerosol phase. This does not explain the observed day time columns NH_3 maximum, which was not observed at the surface. This suggests that T and RH may not be the only driver regarding the vertical
385 variability in NH_3 concentrations. Other possible drivers are analysed in the coming sections.

3.4 Link between ammonia and ammonium particles over the Paris region

A joint analysis of the temporal evolution of ammonia and ammonium particles provides further evidence on the role of particle/gas conversion on the evolution of ammonia concentrations. As previously mentioned,
390 volatilization leads to concomitant increases of ammonia concentrations and decreases of NH_4NO_3 particles (the most abundant ammonium particles observed during this event, Petit et al., 2015). Complementary, the formation of ammonium nitrate particles may be accompanied by a relative reduction of the abundance of its precursors (if they are not in excess), thus ammonia and HNO_3 . The following two subsections analyze these processes for the periods 1 and 2.

395 3.4.1 Local pollution regime on 26-27 March 2012 (period 1)

Figure 7 presents hourly median measurements of ammonia total column from OASIS and surface concentrations of ammonia, ammonium (NH_4^+), nitrate (NO_3^-) and sulfate (SO_4^{2-}) radicals measured at the SIRTa site (respectively in Figs 7a, c, e, for P1 and 7b, d, f, for P2). During P1, hourly ammonia total columns measured by OASIS show a stable level around $2 \cdot 10^{16}$ molec. cm^{-2} until 10:00 UTC, after which a steady increase with larger
400 variability is observed during all the afternoon until reaching a median maximum of $3.4 \cdot 10^{16}$ molec. cm^{-2} around 15:00 UTC (Figure 7a). Surface ammonia concentrations strongly vary during the night and clearly increase in the morning hours with a relative maximum around 07:00 UTC up to $7 \mu\text{g m}^{-3}$, likely related to evaporation from morning dew (Petit et al. 2015; Wentworth et al., 2016) and it is followed by a steady decrease of about 35 % down to $4.5 \mu\text{g m}^{-3}$ around 13:00 UTC. A second relative enhancement of surface NH_3 is seen during the afternoon
405 at 17:00 UTC until reaching $6 \mu\text{g m}^{-3}$, after which it fluctuates with concentrations around $5 \mu\text{g m}^{-3}$ until midnight (Figure 7c). Hourly concentrations of NH_4^+ and NO_3^- show a similar evolution during the day (Figs. 7c, e). They remain rather stable during the night and early morning hours until 06:00 UTC (around ~ 5 and $\sim 18 \mu\text{g m}^{-3}$ for respectively NH_4^+ and NO_3^-), with a relative peak at 03:00 UTC. Afterwards, their concentrations show a small relative peak at 07:00 UTC, followed by a strong reduction of 75 % during the day. Between noon and 19:00
410 UTC, a rather stable daily minimum is seen for both ammonium and nitrate concentrations (of respectively ~ 1 and $\sim 3 \mu\text{g m}^{-3}$). This is followed by a slightly increase (up to 3 and $7 \mu\text{g m}^{-3}$ respectively). Meanwhile, sulfate amounts remain low during P1 (below $1.5 \mu\text{g m}^{-3}$, Fig. 7e).

From the early morning until the afternoon, the strong reduction of 75 % for both ammonium and nitrate abundances at the surface, which is not clearly observed for surface ammonia (reducing by only 35 %), likely
415 suggest the occurrence of volatilization of ammonium particles. Probably, particle volatilization may be observable locally at the Paris region as this first period (P1) is characterized by a rather local pollution regime with limited transport of pollutants from other regions. Sustained volatilization of ammonium particles would lead to a steady enhancement of ammonia concentrations, as it is clearly observed during almost all daytime by OASIS



in terms of NH_3 total columns. An additional factor contributing to the daytime increase of ammonia amounts
420 would be the volatilization of applied mineral fertilizers in the sown crop areas, although additional
measurements in these areas are needed in order to confirm this.

The fact that the daytime enhancement of NH_3 is not that clearly reflected by its variability at surface level (Fig.
7c) might be associated with an additional phenomenon that would reduce surface concentrations of gases and
particles during daytime, such as vertical mixing within the atmospheric boundary layer (which is investigated in
425 detail in Sect. 3.5). Volatilization of ammonium particles is also favored by rather dry conditions during the day,
with surface relative humidity dropping down to 19 % at about 12:00 UTC, while the deliquescence relative
humidity point is 65 % (Fig. 8c). Local meteorological conditions are also characterized by a gentle to fresh
breeze, according to the Beaufort scale, with a dominant wind direction from the north (see Figs. 8e and 8g) and
surface temperatures ranging from 11 to 21°C.

430 **3.4.2 Pollution transported from the Benelux region and west Germany on 28-30 March 2012 (period 2)**

The P2 is characterized by the arrival of polluted air masses to the Paris region, originating from the Benelux and
west Germany region (as remarked in Sect. 3.1, Fig. 3c, f, i) by rather weak winds (2.5 m s^{-1} , Fig. 8f) from the
north and northeast (Fig. 8h). Locally, meteorological conditions favor particle formation during the night
435 (maximum of RH of 95 % above a DRH of 67 %, Fig. 8d) and volatilization during the day (minimum of RH of
27 % well below the DRH of 66 %). A clear and stronger afternoon enhancement of ammonia total columns is
observed (Fig. 7b) as compared to the two previous days (P1, Fig. 7a). The median diurnal evolution of ammonia
columns during P2 depict an early decrease from $1.5 \cdot 10^{16} \text{ molec.cm}^{-2}$ at 07:00 UTC down to $1 \cdot 10^{16} \text{ molec.cm}^{-2}$ at
10:00 UTC. Then, they steadily rise for 6 hours until reaching $3.5 \cdot 10^{16} \text{ molec.cm}^{-2}$ at 16:00 UTC (Fig. 7b) with
440 clearly more variability than during P1. Surface measurements of NH_3 during the night show a steady decrease
from $5 \mu\text{g m}^{-3}$ at midnight to $3 \mu\text{g m}^{-3}$ at 05:00 UTC, with smaller variability as compared to the same period of
the day during P1. Surface NH_3 concentrations increase during the morning until reaching a maximum of $5.7 \mu\text{g m}^{-3}$
at 08:00 UTC, followed by a reduction down to $4 \mu\text{g m}^{-3}$ two hours after (10:00 UTC) and then a second
relative maximum of smaller amplitude ($5 \mu\text{g m}^{-3}$) in the afternoon (15:00 UTC, Fig. 7d). When it comes to the
445 particle components at surface level, all inorganics (ammonium, nitrate and sulfate) exhibit relatively large
amounts and follow similar diurnal evolutions, which is probably associated with the arrival of air pollutants rich
in nitrate (Fig. 7f; also remarked by Petit et al., 2015) from the Benelux and west Germany (Fortems-Cheiney et
al. 2016). The concentrations of these three particle components steadily increase during the night until reaching
a maximum at 07:00 UTC (of 31, 10 and $2.3 \mu\text{g m}^{-3}$ respectively for nitrate, ammonium and sulfate), after which
450 they decrease until 11:00 UTC. Between midnight and 05:00 UTC, the concomitant increase of the abundance of
particle concentrations with a decrease in ammonia amounts might be associated with gas-to-particle conversion
process favored by high relative humidity and low temperatures (see Fig. 8b and 8d) or eventually with the
variability of particle concentrations being advected to the Paris region. In the afternoon, a second relative
maximum of particle component concentrations at the surface is found around 12:00-13:00 UTC, but with lower
455 intensity (19, 6 and $1 \mu\text{g m}^{-3}$ respectively for nitrate, ammonium and sulfate). An evening peak is also remarked
around 22:00 UTC for the concentrations the 3 particle species (respectively 23, 7 and $2 \mu\text{g m}^{-3}$). The daily
evolution after 10:00 UTC of the particle components and ammonia is rather similar, without any particular
anticorrelation which does not suggest a dominant formation or volatilization of particles.



3.5 Vertical distribution of air pollutants over the Paris region

460 In this subsection, we use vertical profiles of aerosol distributions measured by a backscatter lidar at SIRTA in order to analyze the link between air pollutant concentrations at the surface, their vertical profile and total column integrated amounts. Aerosol vertical distribution is used here as a proxy for air pollution, since no measurements of the diurnal evolution of the vertical profiles of gaseous pollutants such as ammonia or specific particle components such as ammonium or nitrate are available (only possible through very specific field deployments
465 such as airborne in situ instrumentation or with a diode laser spectrometer on-board weather or tethered balloons with open cavity, for avoiding the problems of “sticky” nature for ammonia). We depict the average diurnal evolution over the periods P1 and P2, in terms of lidar measurements, sun photometer-derived AODs and surface $PM_{2.5}$ (see Fig.9a-d). Moreover, we extract the time series of lidar attenuated backscatter at 150 m of altitude (the lowest level at which calibrated lidar measurements are available) for depicting the hourly evolution of near
470 surface air pollutant content (Fig. 9e-f, blue curves) and also we use attenuated backscatter integrated (indicated as IAB - Integrated Attenuated Backscatter) over the altitude range from 150 m to 2.5 km for analyzing the corresponding variability of total column amounts (note that no aerosol layers are observed above 2.5 km, Fig. 9e-f, red curves).

During P1 (27-28 March), baseline aerosol load conditions prevail over the Paris region, with an overall low AOD
475 of both fine (~ 0.1) and coarse (~ 0.04) particle fractions (see fine mode AOD at SIRTA in Fig. 9a). This is also shown by lidar measurements, showing attenuated backscatter below 2.5 km of altitude (where particles are located) ranging from $2.5 \text{ Mm}^{-1} \text{ sr}^{-1}$ during the day up to a night maximum of $4.3 \text{ Mm}^{-1} \text{ sr}^{-1}$ near the surface (Fig. 9c, e). According to the evolution of both attenuated backscatter at 150 m and surface $PM_{2.5}$ concentrations, near surface aerosol loads display a relative maximum from 07:00 to 10:00 UTC (thus during the morning peak of road
480 traffic at the Paris megacity; Fig. 9a, e). This is followed by a progressive reduction of near-surface particle amounts from 10:00 UTC until 13:00 UTC, as the atmospheric mixing boundary layer grows from a depth of ~ 400 m at 10:00 UTC up to ~ 1400 m at 13:00 UTC (shown as a magenta dashed line Fig. 9c). A late afternoon aerosol load increase from 16:00 UTC until 19:00 UTC is also depicted by both integrated amounts (particularly backscatter) and near the surface (a small relative maximum), which corresponds to the time of the evening peak
485 of road traffic. The attenuated backscatter integrated from 0.15 to 2.5 km show two additional distinct peaks at 07:00 UTC and 19:30 UTC of about $5.2 \text{ Mm}^{-1} \text{ sr}^{-1}$, which are associated with enhancements of aerosol content from 700 m up to 1500 m of altitude (probably due to horizontal advection, Fig. 9c).

As previously remarked, P2 is characterized by a strong increase in particle load due to transboundary transport of pollution from the Benelux and west Germany (Fig. 3c, f, i). This is reflected by large enhancements of the
490 AOD, surface $PM_{2.5}$ and lidar backscatter (Figs. 9b, f) as compared to P1. An increase of a factor 3 of the fine mode fraction of the AOD (up to ~ 0.29 and ~ 0.32 in Paris and SIRTA, respectively) is observed, while the AOD coarse fraction remains stable (~ 0.04 and ~ 0.03 respectively in Paris and SIRTA, not shown in the figures). Integrated attenuated backscatter and surface $PM_{2.5}$ during P2 are about a factor ~ 2 greater than in the two previous days (P1). After a reduction from 07:00 to 11:00 UTC (also observed for ammonia total columns on 30
495 March, Fig.5a), integrated attenuated backscatter shows a steady hourly enhancement from 12:00 UTC until 19:00 UTC, when it displays a clear evening peak. This steady increase is also measured in terms of AOD, but in this case during all daytime (from 07:00 to 17:00 UTC). This sustained increase during the daytime for vertically



integrated amounts of particles is similar to that observed for the vertically integrated amount of ammonia measured by OASIS (Fig. 7b). Meanwhile, the near surface evolution of particle content shown by both attenuated
500 backscatter at 150 m of altitude and surface $PM_{2.5}$ is clearly different from that of the total amount of particles (respectively blue and red curves in Fig. 9b, f). Near surface aerosol amounts depict both the morning (clearly marked for surface $PM_{2.5}$) and evening relative maxima, that may be associated with road traffic. The reduction of lidar backscatter at 150 m at 07:30 UTC is likely associated with downward mixing of cleaner air (with less aerosols) from the residual layer (Fig. 9d at 07:30 UTC above 200 m) above the mixing boundary layer. The
505 afternoon minor reduction of particles coincides with a slight increase in wind speed leading to vertical and horizontal mixing. An enhancement of particle amounts near the surface is only seen late in the afternoon (around 17:00-18:00 UTC). Surface ammonia concentrations also depicts a similar evolution, depicting the morning and evening peaks, this last one only late in the afternoon. This confirms the consistency of the differences between near surface and total amounts of particle concentrations with those between surface and total column ammonia.

510 The lidar profile time series reveals the link between surface and vertically integrated amounts of aerosols. It clearly depicts the typical diurnal cycle of the atmospheric boundary layer, with a growth of the mixing boundary layer from ~ 150 m at 06:00 UTC until ~ 1500 m at 14:00 UTC (see magenta dashed line in Fig. 9d, likely associated with turbulence generated by sun light surface heating). Turbulence-associated vertical dilution within the mixing boundary layer is most likely a major reason for the clear reduction of near surface concentrations of
515 particles between 06:00 and 14:00 UTC (and we expect the same behavior for surface NH_3 also mixed within the boundary layer). This reduction is not remarked for vertically integrated amounts (AOD, attenuated backscatter or total column NH_3) since a change in the vertical distribution does not affect the total atmospheric amount. We assume that relatively large vertically-integrated amounts of particles between 00:00 UTC and 07:00 UTC in P2 period (compared to P1) are likely linked to particle formation. This is consistent with the relative humidity
520 conditions (maximum of RH of 95 % above DRH of 67%, Fig. 8d) and also the low NH_3 total columns measured by OASIS in the early morning (07:00 UTC) during P2 period (see Fig. 7b and Fig. 5a, showing this last one early morning total columns of NH_3 on 28-29 March smaller than the previous days).

Moreover, it is worth mentioning that although similarly affected by vertical mixing, the evolution of integrated amounts of ammonia and particles are not necessarily linked to the same phenomena. Indeed, the sustained
525 daytime or afternoon enhancement of particle total atmospheric amounts (AOD and integrated attenuated backscatter) during P2 is more likely associated with the advection of larger amounts of particle pollution during the afternoon or particle formation processes, but not to volatilization (which is a sink of particles). However, the afternoon enhancement of ammonia may be reinforced by volatilization during the afternoon drier conditions (see Fig. 8d) and likely also horizontal advection of polluted air masses.

530 Finally, local/regional emission sources could be a possible explanation for the observed afternoon. Agricultural NH_3 emissions are weak over the Greater Paris area, but they are strong over the adjacent Picardie and Ardenne-Champagne regions, located 30 to 150 km upwind of the Créteil measurement site for the north-easterly wind conditions during the P1 and P2 periods (Fortems-Cheiney et al., 2020, Fig. 4c based on detailed emission modelling). The diurnal NH_3 emission variation is strongly temperature dependent as shown among others by
535 Hamaoui-Laguel et al., (2014) from simulations with a mechanistic emission model (Volt'Air, Générumont et al., 2018). Advection of these emissions to the Créteil site could be rapid enough to explain the observed afternoon NH_3 column increase, given the surface wind speed of 3 to 5 m/s and probably larger winds at altitude.



4. Conclusions

540 We have carried out a comprehensive analysis of the diurnal evolution of ammonia amounts at the surface and
over the total atmospheric column during a springtime pollution outbreak at the Paris megacity, considering
different factors and variables that influence their variability at surface level and in altitude. Using remote sensing,
meteorological and chemistry-transport models, we have described the regional atmospheric conditions over
western Europe affecting air quality over the Paris region during late spring 2012. A clear picture of particulate
545 pollution within the Paris region was drawn from in situ surface measurements of PM from the Paris region
operational network. These results allowed us to distinctly identify two phases within the pollution outbreak in
Paris: local formation of rather moderate pollution on 26-27 March 2012 (P1) and the arrival of relatively large
amounts of transboundary pollution from the Benelux and west Germany on 28-30 March 2012 (P2), leading to
high surface PM_{2.5} concentrations (up to 80 µg m⁻³).

550 The daily evolution of ammonia in the Paris megacity was characterized by state-of-the-art measurements from
the AiRRmonia surface in situ instrumentation and remote sensing of total atmospheric columns from the OASIS
observatory. To the authors' knowledge, this is the first study analysing the daily evolution of ammonia total
columns with high temporal resolution (10 minutes in cloud free conditions) over a megacity. Clearly different
evolutions of ammonia concentrations at the surface and integrated over the atmospheric column were observed.
555 Ammonia total columns during the late March 2012 pollution event depicted a clearly steady diurnal enhancement
on each of the days of the event, during most of daytime (2 days) or the afternoon (3 days). On the other hand,
surface ammonia measurements during this event principally revealed rather moderate fluctuations with
significant morning time peaks.

Despite a wide variety of factors influencing ammonia, our study distinctly identifies a crucial role of vertical
560 mixing within the atmospheric boundary layer for explaining the difference between the evolution of ammonia at
the surface and that integrated over the total column. Indeed, the growth of the mixing boundary layer from 150
m deep at 06:00 UTC up to 1500 m deep at 14:00 UTC entrains vertical dilution of atmospheric pollutants within
the boundary layer and thus a relative reduction of air pollutants concentrations near the surface (but not over the
total atmospheric column). By comparing surface (or near surface) and total column amounts, we observe a similar
565 behaviour for both ammonia and particles. Both for P1 and P2, surface concentrations for these two pollutants
mainly depict only morning and late afternoon peaks, while total columns show a steady enhancement particularly
in the afternoon. Vertical dilution is then likely responsible for a prevailing reduction of surface concentrations
until 14:00 UTC (explaining that they do not depict enhancements) and the afternoon enhancement for surface
amounts is only seen later in the afternoon (16:00-17:00 UTC). Moreover, the joint analysis of the evolution of
570 ammonia, ammonium and nitrate highlighted the occurrence of volatilization of these last two to release ammonia
in the atmosphere during the afternoon of P1. When it comes to P2, the evolution of total column amounts of
ammonia and particles in the Paris region seems to be mainly driven by the arrival of polluted air masses
originating from the Benelux. Low relative humidity (clearly below the deliquescence point of ammonium nitrate)
during the afternoons of the last period also suggests the possible volatilization for enhancing ammonia
575 concentration (although this is not clearly seen as a major driver of measured nitrate/ammonium concentrations).
However, the diurnal variation of NH₃ emissions could be one of the factors leading to afternoon maxima, as



emission sources are strong in the vicinity and upwind (under given conditions) of the Paris region. Night time ammonia and ammonium during P2 indicates gas-to-particle formation, which could also occur at higher altitudes (due to higher relative humidity, not shown), leading to distinct lower total column values of ammonia in the early morning (for 2 days). This could also be linked to enhanced HNO₃ transport in the polluted plume.

Our comprehensive study illustrates the benefit of using together total column and surface measurements of ammonia for understanding how vertical mixing within the atmospheric boundary layer influence the daily evolution of ammonia. This work also confirms the role of temperature and relative humidity for ammonia volatilization and particle formation.

For a particular geographical location, ground-based instruments in urban sites such as OASIS with high temporal resolution provide highly valuable information on the diurnal evolution of atmospheric species (especially gaseous pollutants). Ground-based remote sensing is also very valuable for validating satellite retrievals since both typically derive total column amounts of atmospheric species, which may significantly differ from their abundance at the surface.

The results of this study highlight the need of a better chemical characterization for comprehensive understanding of partitioning. Moreover, the vertical distribution of ammonium nitrate partitioning would need to be better constrained versus altitude. This may be addressed, for instance, by the development of spectroscopic instrumentation onboard standard weather or tethered balloons, capable of simultaneously measuring the vertical distribution of ammonia and particles components, in combination with chemistry transport models, as already developed for greenhouse gases (such as CO₂, CH₄ and H₂O, see Joly et al., 2020).

Author contribution

RDK is the main author of the paper, wrote the text, made most of the figures and analyzed the data. JC, PC, JEP and MB contributed to the manuscript writing, discussions and analysis of the figures. JC made one of the figures of the paper. JEP provided data and carried out the ISORROPIA II calculations. PC, MR and XL operated the OASIS observatory. BT made an initial analysis of OASIS data. JCD provided observational data and AR the ESMERALDA/CHIMERE outputs. FH and JO provided support on the analysis and the PROFFIT code for processing OASIS dataset and deriving NH₃ data.

Competing interests

The authors declare that they have no conflict of interest.

Acknowledgments

The authors from LISA acknowledge support from CNES (Centre National des Etudes Spatiales) and the INSU/CNRS (Institut National des Sciences de l'Univers/Centre National de Recherche Scientifique) in the framework of the projects IASI-TOSCA (Terre Ocean Surface Continental Atmosphère) and LEFE-CHAT as well as the OSU-EFLUVE (Observatoire des Sciences de l'Univers-Enveloppes Fluides de la Ville à



l'Exobiologie) and the University Paris Est Créteil for the routine operation of the OASIS observatory. The research was also funded by DIM Qi2 (Paris Region). A particular acknowledgement shall be given to the collaborator of the KIT in Karlsruhe, Germany, for their continues support and involvement. Work at IMK has
615 been funded by the ATMO program of the Helmholtz Association of Germany Research Centres. The authors wish to thank AirParif and SIRTA for in-situ data and ground-based lidar measurements, and the NASA Goddard Space Flight Center for providing the temperature and pressure profiles of the National Centers for Environmental Prediction (NCEP) for the OASIS retrievals of NH₃. Furthermore, our thanks extend to AIRPARIF and their provision of the ESMERALDA output based on CHIMERE, used in this analysis, as well as the IPSL, providing
620 the ERA-Interim reanalysis data that are accessible via the CLIMSERV platform by download. Thanks is extended to the NASA Terra MODIS for providing data on their platform as well as the French data government website, which provided shape files of the land use and were visualized with the Q-GIS software. Finally, the authors want to acknowledge and thank AERONET for the provision of the sun photometer data.

References

- 625 Behera, S. N., Sharma, M., Aneja, V. P., and Balasubramanian, R.: Ammonia in the atmosphere: a review on emission sources, atmospheric chemistry and deposition on terrestrial bodies, *Environ. Sci. Pollut. Res. Int.*, 20(11):8092-131, <https://doi.org/10.1007/s11356-013-2051-9>, 2013.
- Chelin, P., Viatte, C., Ray, M., Eremenko, M., Cuesta, J., Hase, F., Orphal, J., and Flaud, J.-M.: The OASIS Observatory Using Ground-Based Solar Absorption Fourier-Transform Infrared Spectroscopy in the Suburbs of
630 Paris (Créteil-France), *Environmental, Energy and Climate Change I Environmental Chemistry of Pollutants and Wastes*, Springer-Verlag Berlin Heidelberg, 21-52, doi:10.1007/698_2014_270, 2014.
- Clerbaux, C., Boynard, A., Clarisse, L., George, M., Hadji-Lazaro, J., Herbin, H., Hurtmans, D., Pommier, M., Razavi, A., Turquety, S., Wespes, C., and Coheur, P.-F.: Monitoring of atmospheric composition using the thermal infrared IASI/MetOp sounder, *Atmos. Chem. Phys.*, 9, 6041–6054, <https://doi.org/10.5194/acp-9-6041-2009>,
635 2009.
- Cortinovis, J., F. Moreto, A. Yahyaoui, A. Sauvage and L. Letinois : Élaboration d'un cadastre d'émissions interrégional pour la plate-forme de modélisation de prévisions cartographiques ESMEALDA, *Pollution atmosphérique [En ligne]*, 189, URL : <http://lodel.irevues.inist.fr/pollution-atmospherique/index.php?id=1503>, <https://doi.org/10.4267/pollution-atmospherique.1503>, 2015
- 640 Cowen, K., Summer, A. L., Dindal, A., Riggs, K., Willenberg, Z., Hatfield, J., Pfeiffer, R., and Scoggin, K.: *Environmental Technology Verification Report ETV Advanced Monitoring Systems Center Mechatronics Instruments BV AiRRmonia Ammonia Analyzer*, Battelle in cooperation with U.S. Department of Agriculture, under a cooperative agreement with U.S. Environmental Protection Agency, 2004.
- Dammers, E., Shephard, M. W., Palm, M., Cady-Pereira, K., Capps, S., Lutsch, E., Strong, K., Hannigan, J. W.,
645 Ortega, I., Toon, G. C., Stremme, W., Grutter, M., Jones, N., Smale, D., Siemons, J., Hrpcek, K., Tremblay, D., Schaap, M., Notholt, J., and Erisman, J. W.: Validation of the CrIS fast physical NH₃ retrieval with ground-based FTIR, *Atmos. Meas. Tech.*, 10, 2645–2667, <https://doi.org/10.5194/amt-10-2645-2017>, 2017.
- De Mazière, M., Thompson, A. M., Kurylo, M. J., Wild, J. D., Bernhard, G., Blumenstock, T., Braathen, G. O., Hannigan, J. W., Lambert, J.-C., Leblanc, T., McGee, T. J., Nedoluha, G., Petropavlovskikh, I., Seckmeyer, G.,
650 Simon, P. C., Steinbrecht, W., and Strahan, S. E.: The Network for the Detection of Atmospheric Composition



- Change (NDACC): history, status and perspectives, *Atmos. Chem. Phys.*, 18, 4935–4964, <https://doi.org/10.5194/acp-18-4935-2018>, 2018.
- Elster, M., El-Haddad, I., Maasikmets, M., Bozzetti, C., Wolf, R., Ciarelli, G., Slowik, J. G., Richter, R., Teinemaa, E., Hüglin, C., Baltensperger, U., and Prévôt, A. S. H.: High contributions of vehicular emissions to ammonia in three European cities derived from mobile measurements, *Atmospheric Environment* 175, 210-220, <https://doi.org/10.1016/j.atmosenv.2017.11.030>, 2018.
- Fortems-Cheiney, A., Dufour, G., Hamaoui-Laguél, L., Foret, G., Siour, G., Van Damme, M., Meleux, F., Coheur, P.-F., Clerbaux, L., Clarisse, L., Favez, O., Wallasch, M., and Beekmann, M.: Unaccounted variability in NH₃ agricultural sources detected by IASI contributing to European spring haze episode, *Geophys. Res. Lett.*, 43, 5475–5482, doi:10.1002/2016GL069361, 2016.
- Fortems-Cheiney, A., Dufour, G., Dufossé, K., Couvidat, F., Gilliot, J.-M., Siour, G., Beekmann, M., Foret, G., Meleux, F., Clarisse, L., Coheur, P.-F., Van Damme, M., Clerbaux, C., and Générumont, S.: Do alternative inventories converge on the spatiotemporal representation of spring ammonia emissions in France?, *Atmos. Chem. Phys.*, 20, 13481–13495, <https://doi.org/10.5194/acp-20-13481-2020>, 2020.
- Générumont, S., Ramanantenasoa, M. M. J., Dufosse, K., Maury, O., Mignolet, C., and Gilliot, J.-M.: Data on spatio-temporal representation of mineral N fertilization and manure N application as well as ammonia volatilization in French regions for the crop year 2005/06, *Data in Brief*, 21, 1119-1124, <https://doi.org/10.1016/j.dib.2018.09.119>, 2018.
- Giles, D. M., Sinyuk, A., Sorokin, M. G., Schafer, J. S., Smirnov, A., Slutsker, I., Eck, T. F., Holben, B. N., Lewis, J. R., Campbell, J. R., Welton, E. J., Korkin, S. V., and Lyapustin, A. I.: Advancements in the Aerosol Robotic Network (AERONET) Version 3 database – automated near-real-time quality control algorithm with improved cloud screening for Sun photometer aerosol optical depth (AOD) measurements, *Atmos. Meas. Tech.*, 12, 169-209, <https://doi.org/10.5194/amt-12-169-2019>, 2019.
- Guo, H., Otjes, R., Schlag, P., Kiendler-Scharr, A., Nenes, A., Weber, R. J.: Effectiveness of ammonia reduction on control of fine particle nitrate. *Atmos. Chem. Phys.*, 18, 16, <https://doi.org/10.5194/acp-18-12241-2018>, 2018.
- Haefelin, M., Barthès, L., Bock, O., Boitel, C., Bony, S., Bouniol, D., Chepfer, H., Chiriaco, M., Cuesta, J., Delanoë, J., Drobinski, P., Dufresne, J.-L., Flamant, C., Grall, M., Hodzic, A., Hourdin, F., Lapouge, F., Lemaître, Y., Mathieu, A., Morille, Y., Naud, C., Noël, V., O'Hirok, W., Pelon, J., Pietras, C., Protat, A., Romand, B., Scialom, G., and Vautard, R.: SIRTa, a ground-based atmospheric observatory for cloud and aerosol research, *Ann. Geophys.*, 23, 253-275, <https://doi.org/10.5194/angeo-23-253-2005>, 2005.
- Hamaoui-Laguél, L., Meleux, F., Beekmann, M., Bessagnet, B., Générumont, S., Cellier, P., and Létinois, L.: Improving ammonia emissions in air quality modelling for France, *Atmospheric Environment*, 92, 584-595, <https://doi.org/10.1016/j.atmosenv.2012.08.002>, 2012.
- Hase, F., Hannigan, J. W., Coffey, M. T., Goldman, A., Höpfner, M., Jones N. B., Rinsland, C. P., and Wood, S. W.: Intercomparison of retrieval codes used for the analysis of high-resolution, ground-based FTIR measurements, *J. Quant. Spectrosc. Rad. Transf.*, 87, 25–52, <https://doi.org/10.1016/j.jqsrt.2003.12.008>, 2004.
- Holben, B. N., Tanré, D., Smirnov, A., Eck, T. F., Slutsker, I., Abuhassan, N., Newcomb, W. W., Schafer, J. S., Chatenet, B., Lavenu, F., Kaufman, Y. J., Vande Castle, J., Setzer, A., Markham, B., Clark, D., Frouin, R., Halthore, R., Karneli, A., O'Neill, N. T., Pietras, C., Pinker, R. T., Voss, K., and Zibordi, G.: An emerging



- 690 ground-based aerosol climatology: Aerosol optical depth from AERONET, *JGR*, Volume 106, Issue D11, pp. 12,067–12,097, <https://doi.org/10.1029/2001JD900014>, 2001.
- Joly, L., Coopmann, O., Guidard, V., Decarpenierie, T., Dumelié, N., Cousin, J., Burgalat, J., Chauvin, N., Albora, G., Maamary, R., Miftah El Khair, Z., Tzanos, D., Barrié, J., Moulin, É., Aressy, P., and Belleudy, A.: The development of the Atmospheric Measurements by Ultra-Light Spectrometer (AMULSE) greenhouse gas
695 profiling system and application for satellite retrieval validation, *Atmos. Meas. Tech.*, 13, 3099–3118, <https://doi.org/10.5194/amt-13-3099-2020>, 2020.
- Krupa, S. V.: Effects of atmospheric ammonia (NH₃) on terrestrial vegetation: a review, *Environmental Pollution* 124, 179–221, [https://doi.org/10.1016/S0269-7491\(02\)00434-7](https://doi.org/10.1016/S0269-7491(02)00434-7), 2003.
- 700 Levy, R., and Hsu, C.: MODIS Atmosphere L2 Aerosol Product. NASA MODIS Adaptive Processing System, Goddard Space Flight Center, USA: http://dx.doi.org/10.5067/MODIS/MOD04_L2.006 (Terra); http://dx.doi.org/10.5067/MODIS/MYD04_L2.006 (Aqua), 2015.
- Meier, A., Toon, G. C., Rinsland, C. P., Goldman, A. and Hase, F.: A spectroscopic atlas of atmospheric microwindows in the middle infrared, IRF technical report 048, Swedish Institute of Space Physics, 608 pp, id
705 e9e15084-c860-4d1b-8640-4ca2b616a714, 2004.
- Menut, L., Bessagnet, B., Khvorostyanov, D., Beekmann, M., Blond, N., Colette, A., Coll, I., Curci, G., Foret, G., Hodzic, A., Mailler, S., Meleux, F., Monge, J.-L., Pison, I., Siour, G., Turquety, S., Valari, M., Vautard, R., and Vivanco, M. G.: CHIMERE 2013: a model for regional atmospheric composition modelling, *Geosci. Model Dev.*, 6, 981–1028, <https://doi.org/10.5194/gmd-6-981-2013>, 2013.
- 710 Middlebrook, A. M., Bahreini, R., Jimenez, J. L., and Canagaratna, M.R.: Evaluation of Composition-Dependent Collection Efficiencies for the Aerodyne Aerosol Mass Spectrometer using Field Data, *Aerosol Science and Technology*, 46, 258–271, <https://doi.org/10.1080/02786826.2011.620041>, 2012.
- Molina, M. J. and Molina, L. T.: Megacities and Atmospheric Pollution, *Journal of the Air & Waste Management Association*, 54:6, 644–680, DOI: 10.1080/10473289.2004.10470936, 2004.
- 715 Nenes, A., Pandis, S. N., and Pilinis, C.: ISORROPIA: A new thermodynamic equilibrium model for multiphase multicomponent inorganic aerosols, *Aquatic Geochemistry*, 4, 123–152, 1998.
- Ng, N. L., Herndon, S. C., Trimborn, A., Canagaratna, M. R., Croteau, P. L., Onasch, T. B., Sueper, D., Worsnop, D. R., Zhang, Q., and Sun, Y. L.: An aerosol chemical speciation monitor (ACSM) for routine monitoring of the composition and mass concentrations of ambient aerosol, *Aerosol Sci. Tech.*, 45, 780–794, 2011.
- 720 Norman, M., Spirig, C., Wolff, V., Trebs, I., and Flechard, C., Wisthaler, A., Schnitzhofer, R., Hansel, A., and Neftel, A.: Intercomparison of ammonia measurement techniques at an intensively managed grassland site (Oensingen, Switzerland). *Atmospheric Chemistry and Physics*, European Geosciences Union, 9 (8), pp.2635–2645. DOI: 10.5194/acp-9-2635-2009, 2009.
- O’Neill, N. T., Eck, T. F., Smirnov, A., Holben, B. N., and Thulasiraman, S.: Spectral discrimination of coarse and fine mode optical depth, *J. Geophys. Res.*, 108(D17), 4559, doi:10.1029/2002JD002975, 2003.
- 725 Petetin, H., Sciare, J., Bressi, M., Gros, V., Rosso, A., Sanchez, O., Sarda-Estève, R., Petit, J.-E., and Beekmann, M.: Assessing the ammonium nitrate formation regime in the Paris megacity and its representation in the CHIMERE model, *Atmos. Chem. Phys.*, 16, 10419–10440, <https://doi.org/10.5194/acp-16-10419-2016>, 2016.
- Petit, J.-E., Favez, O., Sciare, J., Crenn, V., Sarda-Estève, R., Bonnaire, N., Močnik, G., Dupont, J.-C., Haefelin, M., and Leoz-Garziandia, E.: Two years of near real-time chemical composition of submicron aerosols in the
730



- region of Paris using an Aerosol Chemical Speciation Monitor (ACSM) and a multi-wavelength Aethalometer, *Atmos. Chem. Phys.*, 15, 2985-3005, <https://doi.org/10.5194/acp-15-2985-2015>, 2015.
- Petit, J.-E., Amodeo, T., Meleux, F., Bessagnet, B., Menut, L., Grenier, D., Pellan, Y., Ockler, A., Rocq, B., Gros, V., Sciare, J., Favez, O.: Characterising an intense PM pollution episode in March 2015 in France from multi-site
735 approach and near real time data: Climatology, variabilities, geographical origins and model evaluation, *Atmospheric Environment*, 155, 68-84, <https://doi.org/10.1016/j.atmosenv.2017.02.012>, 2017.
- Ramanantenasoa, M. M. J., Gilliot, J. M., Mignolet, C., Bedos, C., Mathias, E., Eglin, T., Makowski, D., and G nermont, S.: A new framework to estimate spatio-temporal ammonia emissions due to nitrogen fertilization in France, *Science of the Total Environment*, 645, 205–219, <https://doi.org/10.1016/j.scitotenv.2018.06.202>, 2018.
- 740 Remer, L.A., Kaufman, Y.J., Tandr , D., Mattoo, S., Chu, D.A., Martins, J.V., Li, R.-R., Ichoku, C., Levy, R.C., Kleidman, R.G., Eck, T. F., Vermote, E., and Holben, B.N.: The MODIS Aerosol Algorithm, Products, and Validation, *J. Atmos. Sci.*, 62 (4): 947–973, <https://doi.org/10.1175/JAS3385.1>, 2005.
- Sciare, J., d'Argouges, O., Sarda-Est ve, R., Gaimoz, C., Dolgorouky, C., Bonnaire, N., Favez, O., Bonsang, B., and Gros, V.: Large contribution of water-insoluble secondary organic aerosols in the region of Paris (France)
745 during wintertime, *J. Geophys. Res.*, 116, D22203, <https://doi.org/10.1029/2011JD015756>, 2011.
- Seinfeld, J. H. and Pandis, S. N.: *Atmospheric Chemistry and Physics: from Air Pollution to Climate Change*, third ed., John Wiley & Sons, New York, 1121 pp., 2016.
- Serrano, H. C., Oliveira, M. A., Barros, C., Augusto, A. S., Pereira, M. J., Pinhp, P., and Branquinho, C.: Measuring and mapping the effectiveness of the European Air Quality Directive in reducing N and S deposition
750 at the ecosystem level, *Sci. Total Environ.*, 647, 1531-1538, <https://doi.org/10.1016/j.scitotenv.2018.08.059>, 2019.
- Shephard, M. W. and Cady-Pereira, K. E.: Cross-track Infrared Sounder (CrIS) satellite observations of tropospheric ammonia, *Atmos. Meas. Tech.*, 8, 1323–1336, <https://doi.org/10.5194/amt-8-1323-2015>, 2015.
- Simmons, A., Uppala, S., Dee, D., and Kobayashi, S.: ERA-Interim: New ECMWF reanalysis products from 1989
755 onwards, *ECMWF Newsletter*, 110, 25-35, 2007.
- Sommer, S.G., Schjoerring, J., and Denmead, O.: Ammonia Emission from Mineral Fertilizers and Fertilized Crops. *Advances in Agronomy*. 82. 557-622. 10.1016/S0065-2113(03)82008-4, DOI: 10.1016/S0065-2113(03)82008-4, 2004.
- Sutton, A. M., Reis, S., Riddick, S. N., Dragosits, U., Nemitz, E., Theobald, M. R., Tang Y. S., Braban, C. F.,
760 Vieno, M., Dore, A. J., Mitchell, R. F., Wanless, S., Daunt, F., Fowler, D., Blackall, T. D., Milford, C., Flechard, C. R., Loubet, B., Massad, R., Cellier, P., Personne, E., Coheur, P. F., Clarisse, L., Van Damme, M., Ngadi, Y., Clerbaux, C., Skj th, C. A., Geels, C., Hertel, O., Wichink Kruit R. J., Pinder, R. W., Bash, J. O., Walker, J. T., Simpson, D., Horv th, L., Misselbrook, T. H., Bleeker, A., Dentener, F. and de Vries, W.: Towards a climate-dependent paradigm of ammonia emission and deposition, *Phil. Trans. R. Soc. B.*, 368: 20130166.
765 <http://dx.doi.org/10.1098/rstb.2013.0166>, 2013.
- Tournadre, B., Chelin, P., Ray, M., Cuesta, J., Kutzner, R. D., Landsheere, X., Fortems-Cheiney, A., Flaud, J.-M., Hase, F., Blumenstock, T., Orphal, J., Viatte, C., and Camy-Peyret, C.: Atmospheric ammonia (NH₃) over the Paris megacity: 9 years of total column observations from ground-based infrared remote sensing, *Atmos. Meas. Tech.*, 13, 3923–3937, <https://doi.org/10.5194/amt-13-3923-2020>, 2020.



- 770 Van Damme, M., Whitburn, S., Clarisse, L., Clerbaux, C., Hurtmans, D., and Coheur, P.-F.: Version 2 of the IASI NH₃ neural network retrieval algorithm: near-real-time and reanalysed datasets, *Atmos. Meas. Tech.*, 10, 4905–4914, <https://doi.org/10.5194/amt-10-4905-2017>, 2017.
- Van Damme, M., Clarisse, L., Whitburn, S. et al. Industrial and agricultural ammonia point sources exposed. *Nature* 564, 99–103, <https://doi.org/10.1038/s41586-018-0747-1>, 2018.
- 775 Viatte, C., Gaubert, B., Eremenko, M., Hase, F., Schneider, M., Blumenstock, T., Ray, M., Chelin, P., Flaud, J.-M., and Orphal, J.: Tropospheric and total ozone columns over Paris (France) measured using medium-resolution ground-based solar-absorption Fourier-transform infrared spectroscopy, *Atmos. Meas. Tech.*, 4, 2323–2331, <https://doi.org/10.5194/amt-4-2323-2011>, 2011.
- Viatte, C., Wang, T., Van Damme, M., Dammers, E., Meleux, F., Clarisse, L., Shephard, M. W., Whitburn, S.,
- 780 Coheur, P. F., Cady-Pereira, K. E., and Clerbaux, C.: Atmospheric ammonia variability and link with particulate matter formation: a case study over the Paris area, *Atmos. Chem. Phys.*, 20, 577–596, <https://doi.org/10.5194/acp-20-577-2020>, 2020.
- von Bobruzki, K., Braban, C. F., Famulari, D., Jones, S. K., Blackall, T., Smith, T. E. L., Blom, M., Coe, H., Gallagher, M., Ghalaieny, M., McGillen, M. R., Percival, C. J., Whitehead, J. D., Ellis, R., Murphy, J., Mohacsi,
- 785 A., Pogany, A., Junninen, H., Rantanen, S., Sutton, M. A., and Nemitz, E.: Field inter-comparison of eleven atmospheric ammonia measurement techniques, *Atmos. Meas. Tech.*, 3, 91–112, <https://doi.org/10.5194/amt-3-91-2010>, 2010.
- Weber, R. J., Guo, H., Russell, A. G. and Nenes, A.: High aerosol acidity despite declining atmospheric sulfate concentrations over the past 15 years. *Nat. Geos.*, 9.4, 282–285, doi: 10.1038/NGEO2665, 2016.
- 790 Wentworth, G. R., Murphy, J. G., Benedict, K. B., Bangs, E. J., and Collett Jr., J. L.: The role of dew as a night-time reservoir and morning source for atmospheric ammonia, *Atmos. Chem. Phys.*, 16, 7435–7449, <https://doi.org/10.5194/acp-16-7435-2016>, 2016.
- Yokelson, R. J., Christian, T. J., Bertschi, I. T., Hao, W. M.: Evaluation of adsorption effects on measurements of ammonia, acetic acid, and methanol. *J. Geophys. Res. Atmos.*, 108, No. D20, 4649,
- 795 <https://doi.org/10.1029/2003JD003549>, 2003.
- Zhou, M., Langerock, B., Vigouroux, C., Sha, M. K., Ramonet, M., Delmotte, M., Mahieu, E., Bader, W., Hermans, C., Kumps, N., Metzger, J.-M., Dufлот, V., Wang, Z., Palm, M., and De Mazière, M.: Atmospheric CO and CH₄ time series and seasonal variations on Reunion Island from ground-based in situ and FTIR (NDACC and TCCON) measurements, *Atmos. Chem. Phys.*, 18, 13881–13901, <https://doi.org/10.5194/acp-18-13881-2018>,
- 800 2018.



Table 1. Correlation of different available PM values of Vitry, Gennevilliers, Bobigny and SIRTA sites during 26-27 March (period 1) and 28-30 March (period 2). SE refers to Standard Error, and R^2 to the square of the correlation coefficient.

	26-27 March (Period 1)			28-30 March (Period 2)		
	Slope	SE	R^2	Slope	SE	R^2
PM _{2.5} Vitry vs PM _{2.5} Gennevilliers	0.84	0.09	0.67	0.91	0.04	0.86
PM _{2.5} Vitry vs PM _{2.5} Bobigny	0.89	0.10	0.63	0.94	0.04	0.91
PM ₁₀ Vitry vs PM ₁₀ Gennevilliers	1.04	0.09	0.74	1.04	0.05	0.84
PM ₁₀ Vitry vs PM ₁₀ Bobigny	1.02	0.11	0.63	0.93	0.07	0.73
PM ₁ SIRTA vs PM _{2.5} Vitry	0.57	0.06	0.67	0.49	0.08	0.35
PM ₁ SIRTA vs PM _{2.5} Gennevilliers	0.61	0.04	0.82	0.44	0.09	0.26
PM ₁ SIRTA vs PM _{2.5} Bobigny	0.57	0.04	0.84	0.48	0.08	0.34

805



Table 2. Meteorological variables at the surface and AOD on 26-27 March (period 1) and on 28-30 March (period 2), displayed by the median, minimum and maximum values, for temperature, relative humidity, deliquescence relative humidity, wind speed and –direction as well as AOD in its fine mode (FM) and coarse mode (CM).

	Period 1			Period 2		
	Median	Minimum	Maximum	Median	Minimum	Maximum
Temperature (°C)	16.2	10.8	21.8	14.8	10.5	21.0
Relative Humidity (%)	41.8	19.0	66.0	54.8	26.5	77.0
Deliquescence Relative Humidity (%)	70.9	65.1	76.7	72.1	65.6	77.2
Wind speed (m/s)	3.34	0.86	8.19	2.51	0.29	7.09
FM AOD 550nm – Paris	0.10	0.05	0.14	0.29	0.13	0.55
CM AOD 550nm – Paris	0.04	0.02	0.07	0.04	0.02	0.13
FM AOD 550nm – SARTA	0.10	0.04	0.15	0.32	0.10	0.62
CM AOD 550nm – SARTA	0.04	0.01	0.08	0.03	0.02	0.17

810

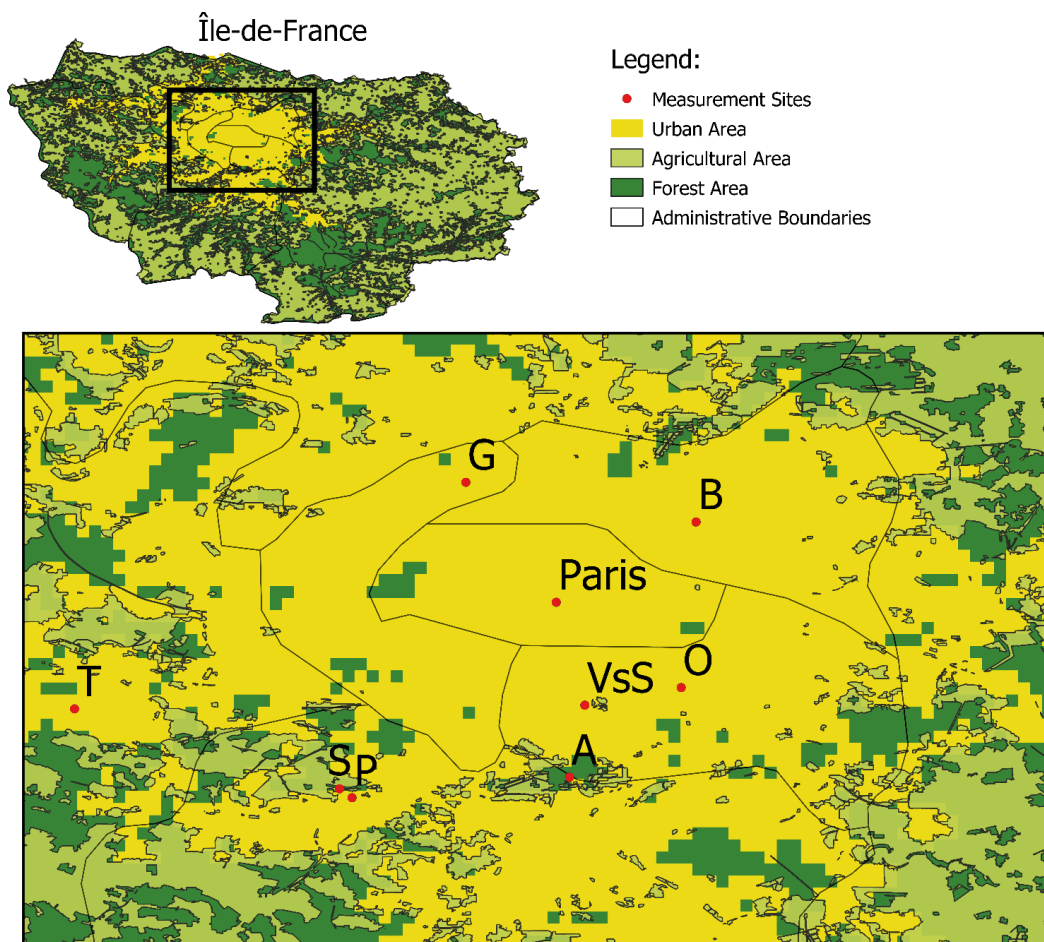
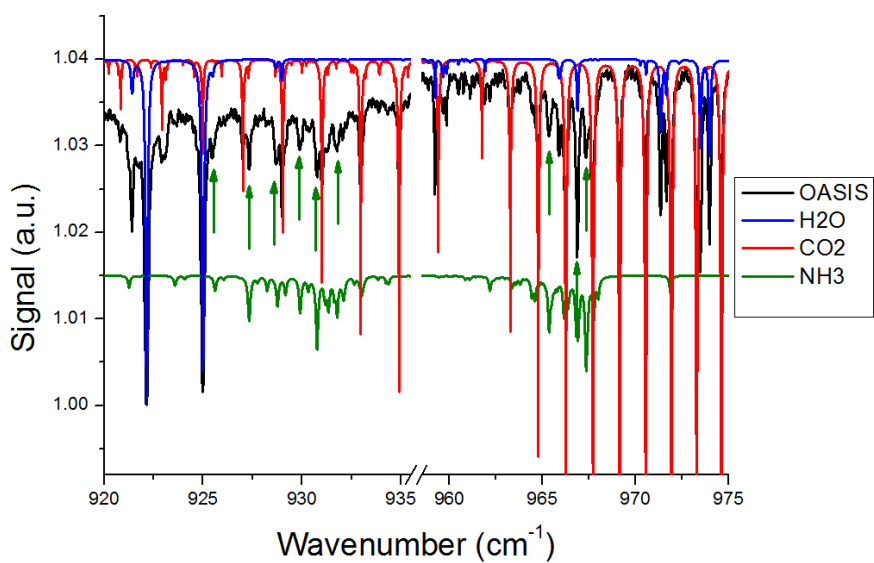
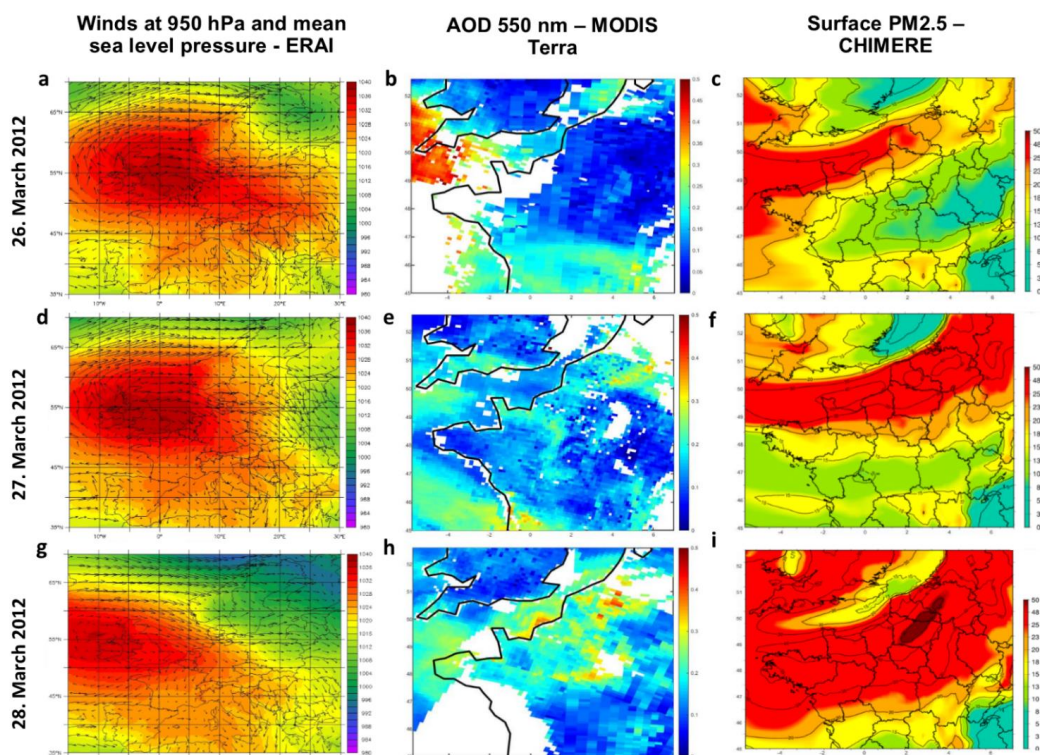


Figure 1. Outline of Paris Region and a zoom into relevant sites (A – Airport Orly, B – Bobigny, G – Gennevilliers, O – OASIS, P – Palaiseau, S – SIRTA, T – Trappes, VsS - Vitry-sur-Seine) using shape files provided by data.gouv.fr (<https://www.data.gouv.fr/fr/datasets/espaces-agricoles-de-la-region-ile-de-france-inscrits-sur-la-cdgt-du-sdrif-arrete-en-2012-idf/#discussion-5cc30bdb8b4c4166219c058e>, last access: 30 April 2019) and processed with QGIS 3.6.

815



820 **Figure 2.** OASIS-FTIR atmospheric spectrum recorded with the BRUKER Vertex 80 at Creteil on 21 March 2012 in the two microwindows (before and after the spectral gap), showing the strong ammonia absorbing lines around $10\ \mu\text{m}$ with individual contributions of the main interfering species represented from the atlas of Meier et al. (2004).



825

Figure 3. (a, d, g) Meteorological conditions characterized by 950 hPa winds (arrows) and sea level pressure (shading) over Europe (15° W to 20°E and 40° to 65°N) from ERAI reanalysis in 26-28 March 2012. Horizontal distribution of particles over northern France (-5° to 7°E and 45° to 52.5°N) in terms of (b, e, h) AOD at 550 nm from MODIS on-board the Terra satellite and (c, f, i) surface PM_{2.5} from the CHIMERE model in the period 26-

830

28 March 2012.

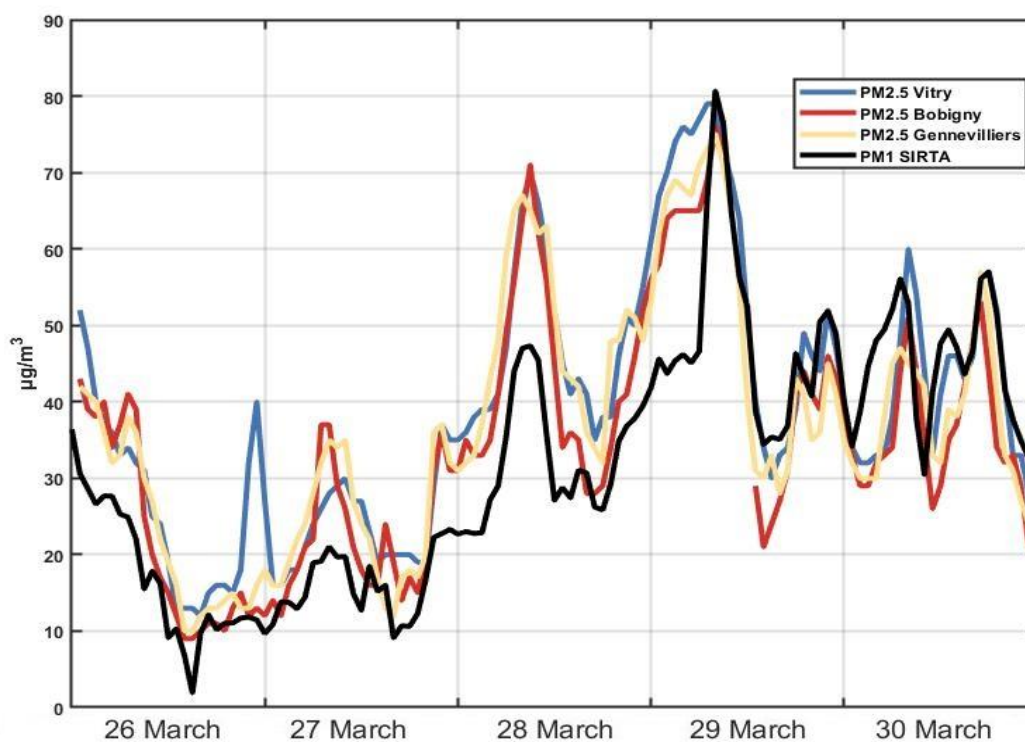
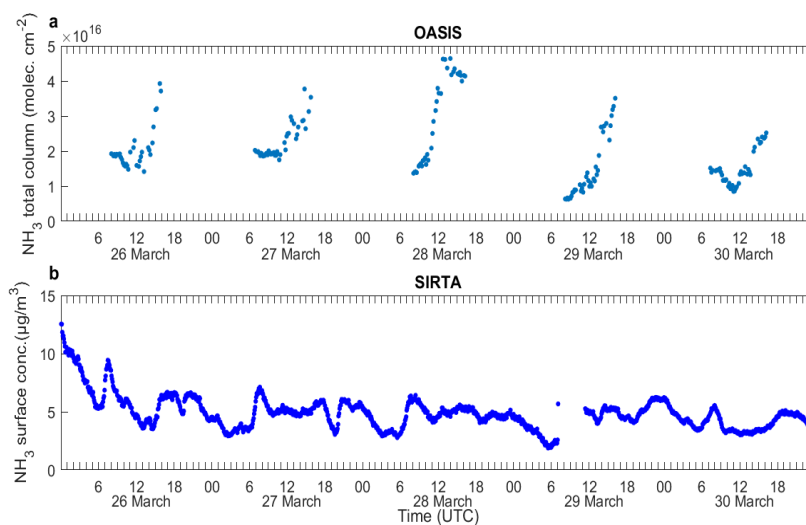
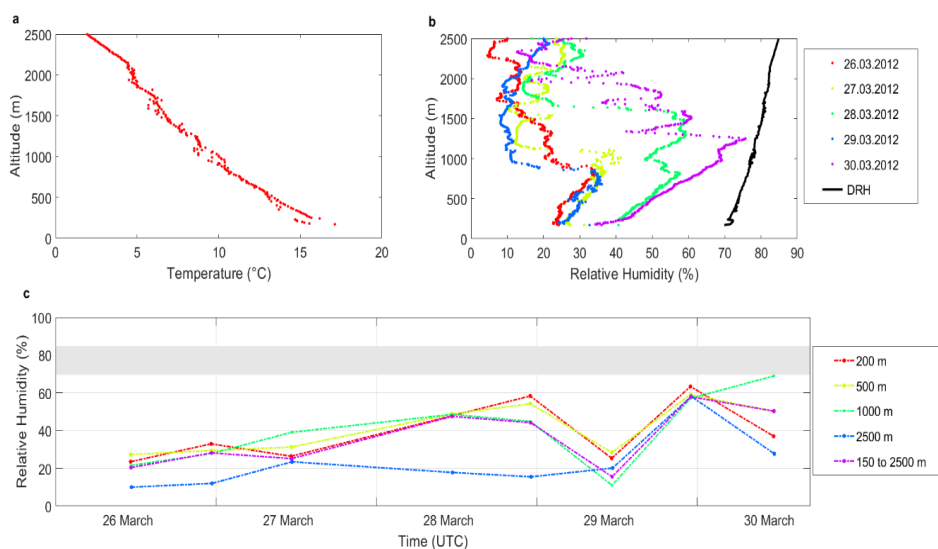


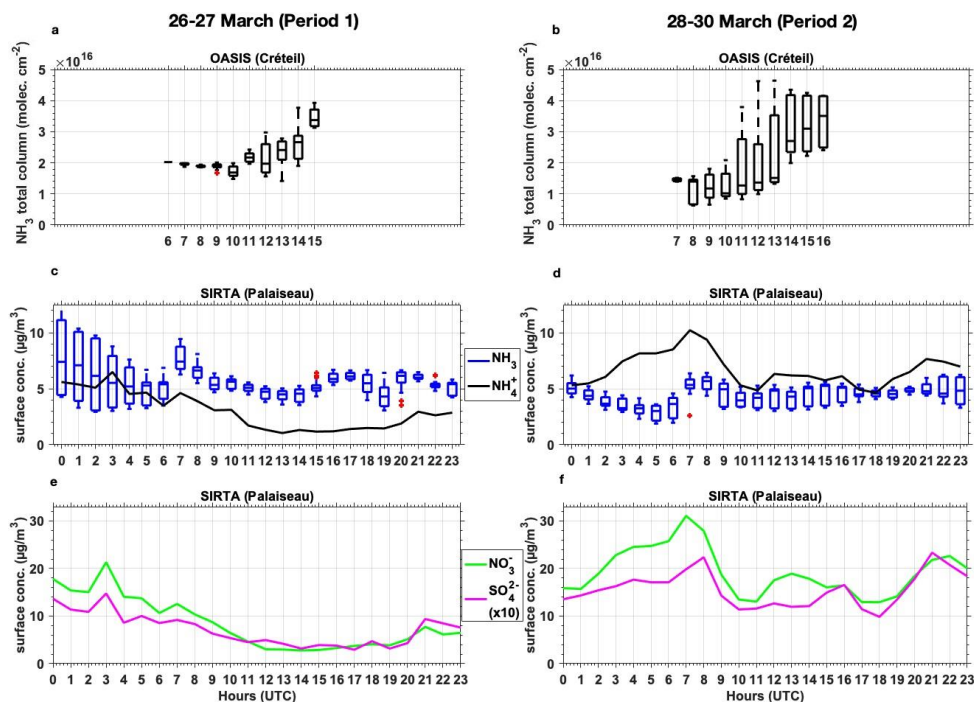
Figure 4. Particle matter concentrations measured at the surface at the station of Vitry, Bobigny, Gennevilliers and Sirta, respectively southeast, northeast, northwest and southwest of Paris. Particle concentrations in terms of $PM_{2.5}$ and PM_1 are provided respectively at the Airparif three stations and at the last one in the period between 26-31 March 2012.



840 **Figure 5.** Observations of atmospheric ammoniac concentrations over the Paris region from 26 to 30 March 2012. The upper panel (a) displays total column retrievals at Créteil derived from OASIS observatory (48.79N 2.44E) measurements during the day (~07:00 and 16:00 UTC). The lower panel (b) displays continued ammonia surface concentration measurements from the AiRRmonia instrument near Palaiseau (SIRT A observatory, 48.71N 2.20E). This figure shows all available individual measurements from OASIS FTIR instrument and AiRRmonia in situ analyser.

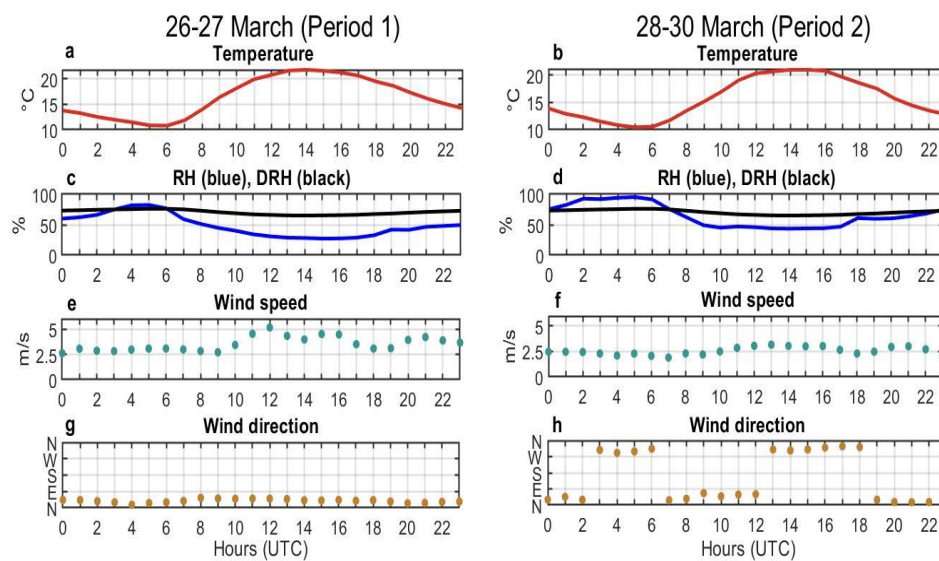


845 **Figure 6.** (a) Median temperature (°C) over the period of interest in the vertical during mid-day. (b) Relative
850 relative humidity (%) in the vertical (mid-day only) from Trappes station and DRH based on the median temperature from
(a). (c) Relative humidity evolution at different heights (average over ± 25 m) for all radio-soundings on 26-30
March, whereby the grey bar indicates the DRH lowest and highest values corresponding to 170 m and 2500 m
altitude. DRH refers to Deliquescence Relative Humidity.



855

Figure 7. Average diurnal evolution of total column NH_3 (a, b), surface NH_3 and NH_4^+ (c, d), hourly median surface measurements of NO_3^- and SO_4^{2-} (e, f) for period 1 on the left side and period 2 on the right side. Hourly boxplots of NH_3 total column retrieved from OASIS (a, b) and hourly boxplots of NH_3 from surface measurements show within the boxplot the median as a line in the plot, 25th and 75th percentile as the lower and upper border of the box and whiskers extended to most extreme data points, whereby outliers are separately marked with a '+'.
860



865 **Figure 8.** Hourly median surface temperature in °C (a, b), relative humidity (blue) and calculated deliquescence relative humidity (DRH; black) in % (c, d), wind speed in m/s (e, f) and wind direction in degrees (g, h) are presented in the left column for period 1 and in the right column for period 2. Whereby temperature and relative humidity measurements origin from OASIS, while wind speed and wind direction origin from SIRTA supersite.



870

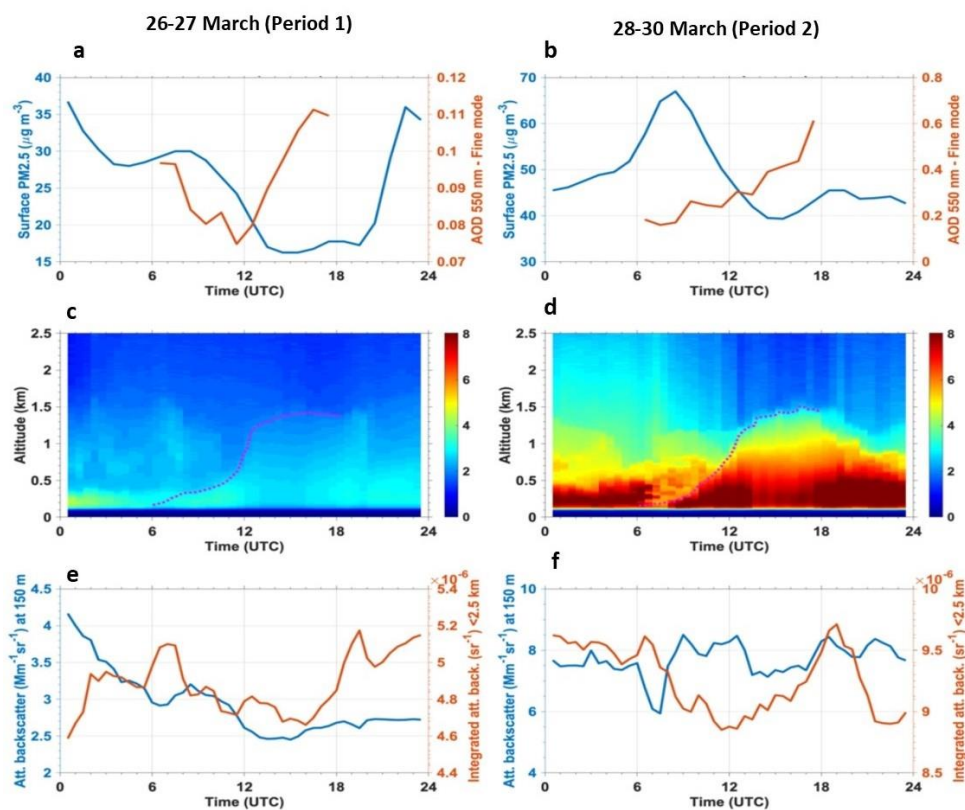


Figure 9. Median diurnal evolution of the AOD of the fine mode fraction of aerosols at 550 nm at SIRTA (red lines) and surface measurements of PM_{2.5} at Vitry (blue lines) during the periods (a) 26-27 March 2012 (P1) and (b) 28-30 March 2012 (P2). Median diurnal evolution of vertical profiles of attenuated backscatter measurements at 355 nm of a ground-based lidar at SIRTA for depicting the vertical distribution of aerosols during (c) P1 and (d) P2. Dashed magenta lines in (c) and (d) show the top of the mixing boundary layer manually tracked as the lowest discontinuity of the lidar profiles during daytime (06:00 – 18:00 UTC). Lidar-derived proxies of the diurnal evolution of particles over the total column (attenuated backscatter integrated between 0.15 and 2.5 km of altitude, in red) and near the surface (attenuated backscatter at 0.15 km, in blue) for (e) P1 and (f) P2. For clarity, measurements in panels (a, b) are shown with hourly time resolution whereas it is of 30 minutes for panels (c-f).